Title
NUCLEAR RELAXATION OF CU63 in Ni-CU

Author
Bancroft, Michael H.

Publication Date
1968-09-01

UCRL-18461

eg. 2

University of California

Ernest O. Lawrence Radiation Laboratory

NUCLEAR RELAXATION OF CU^{63} IN NI–CU

Michael H. Bancroft

(Ph.D. Thesis)

September 1968

Berkeley, California

DISCLAIMER

UCRL-18461

UNIVERSITY OF CALIFORNIA
Lawrence Radiation Laboratory
Berkeley, California
AEC Contract No. W-7405-eng-48

NUCLEAR RELAXATION OF CU^{63} IN NI-CU

Michael H. Bancroft

(Ph.D. Thesis)

September 1968

TABLE OF CONTENTS

NUCLEAR RELAXATION OF Cu^{63} IN Ni-Cu

Michael H. Bancroft

Inorganic Materials Research Division, Lawrence Radiation Laboratory,
Department of Physics, University of California,
Berkeley, California

ABSTRACT

Nuclear magnetic relaxation of Cu^{63} in dilute Ni-Cu alloys has been measured in the temperature range 2.1°K - 300°K. The observed spin echo comes from nuclei in the wings of the domain walls in zero applied field and from nuclei in the saturated bulk in large external field. The longitudinal relaxation rate was found to be proportional to the temperature in both cases. We find T_1T = 0.1 sec. °K and 1.02 ± .10 sec. °K for zero and high external field respectively. The difference between these rates is attributed to a mechanism involving the domain walls. Comparison of the high field rate is made with Moriya's calculation for pure transition metal ferromagnets. It is concluded that there is little or no contribution from the d band to the relaxation of an isolated Cu in Ni. This strongly suggests that a Cu atom in Ni has no local moment. In the helium temperature range, the transverse relaxation is dominated by spin-spin interactions for Cu concentrations as low as 1%.

INTRODUCTION

The origin of ferromagnetism in the 3d transition metals is not yet quantitatively understood. The main problem is the nature of the 3d band. It is mid-way between the nearly free electron and tight binding limits and is therefore hard to deal with. Another complication is the presence of the partly filled 4s band, with which the 3d electrons interact and mix.

One technique for probing the ferromagnetic state is to add impurities to see how they affect the magnetic properties locally and on the average. Much work has been done on alloys of 3d ferromagnetic metals with other transition and noble metals. The macroscopic, or average, effect is shown in the Slater-Pauling diagram, Fig. 1, which plots the saturation magnetization, reduced to average moment/atom, versus electron concentration, for different 3d transition metal alloys. Much of the right hand side of the diagram is explicable in terms of a rigid band model, in which the band structure and resulting density of states remains the same. These bands are merely filled to a different level, depending on the alloy's electron concentration.

An example of this behavior is the alloy Ni-Cu, which has some simplicity from the theoretical viewpoint. These elements adjoin in the periodic table. That they have similar electronic properties is indicated by the fact that they form a complete series of solid solutions. Ni is ferromagnetic, having 0.54 holes in the ↓ (minority spin) d band.[1] Cu is paramagnetic and has a filled d band. Thus in the ferromagnetic Ni-Cu problem, only the 3d ↓ and 4s electrons need be considered. Finally, the band structure of Ni and Cu are accurately known and are

quite similar, which substantiates the rigid band model. In alloys of Ni with less than 40% Cu, the average moment/atom measured is:[2]

$$\bar{\mu} = 0.6 - c_{Cu} \qquad (\text{in } \mu_B)$$

The moment of 0.6 μ_B/atom in pure Ni corresponds to the 0.54 d ↓ holes, when account is taken of the associated orbital moment, which gives rise to the g factor, 2.20, in Ni.[3] The term $-c_{Cu}$ in the equation for $\bar{\mu}$ of Ni-Cu indicates that each Cu atom added reduces the total magnetic moment by one Bohr magneton. This is to be understood in the rigid band model in light of the fact that the density of d states at the Fermi surface in Ni is about ten times that of the s states.[4] Thus, filling up these bands, the extra electron contributed by the Cu goes 9/10 into the d ↓ band and 1/10 into the s band. Again taking account of the Ni's g factor, this filling up of the d ↓ band removes 0.9 x 2.20/2 = 1.0 μ_B from the moment.

Microscopically, of course, the situation is more complex. The extra electron is not distributed uniformly, because of screening. Each Cu, having an extra positive charge, will attract an extra electron to its vicinity. Because of the relative density of states, the screening will be done 90% by the d band, i.e. an isolated Cu ion in Ni will have an extra 0.9 d character electron around it. However, the Cu ion can only accept 0.54 additional 3d electrons before its 3d states are full, i.e. has its full complement of 10 d electrons. Thus the other 0.36 electron must be shared among the Cu impurity's Ni neighbors, thereby reducing their moments. Assuming the screening will take place as locally as possible, the extra 0.36 d electron is shared by the 12 Ni

nearest neighbors. I will call this picture the screening model. It is illustrated in Fig. 2, which is a cross section of an isolated Cu atom in fcc Ni, showing one set of nearest neighbor Ni's and one set of next nearest neighbors, representing distant Ni's. Beneath each atom is the number of holes in its d states in this simple screening model.

We will consider three experiments which give microscopic information about the situation in the vicinity of the impurity: neutron diffraction, n.m.r. or Mössbauer effect, and nuclear relaxation. Neutrons, having a magnetic moment but no charge, sense the electrons only magnetically. By measuring diffuse scattering of neutrons, one can deduce the magnetic moment of an impurity, which introduces non-periodicity, and hence diffuse scattering, if its moment is different from that of the host atoms. By doing n.m.r. in zero external field, that is in the spontaneous field at the nucleus in a ferromagnet,[5] one measures the so called hyperfine field, H_n, at the nucleus involved. Likewise, the splitting of the Mössbauer γ-ray line, due to orientation of the nuclear moment with respect to H_n, measures this field at the nucleus involved.[6] In impurity studies, n.m.r. or Mössbauer effect measures H_n for the host and impurity sites. In addition, H_n of atoms neighboring impurities (either host or other impurity atoms) can be measured by observing satellite lines on the main resonance whose intensity agrees with the number of neighbors and impurity concentration. For instance, from the screening model of Fig. 2, one might expect a satellite line on the low frequency side of the main Ni resonance in a Ni-Cu alloy due to Ni nuclei which are nearest neighbors to an isolated Cu. This is because one would expect a smaller hyperfine field at a site with a smaller moment[7] and hence a lower resonant frequency.

In this work, I have measured nuclear relaxation using the spin echo pulsed n.m.r. technique.[8] This technique consists of applying two r.f. pulses at the n.m.r. frequency and observing a burst of r.f. of the same frequency (the "spin echo") an equal time later. One can understand the main features in terms of the phenomenological Bloch equations, which describe the motion of the macroscopic nuclear magnetization. These contain two parameters: T_1, the longitudinal relaxation time, and T_2, the transverse relaxation time. If one starts the magnetization, M, at some angle to the static field, H_n, it will precess at the resonant frequency. $1/T_1$ is the rate at which M relaxes to the equilibrium position along H_n. $1/T_2$ is the rate for the transverse component of M to dephase microscopically, thus disappearing on a macroscopic scale. One measures T_2 by observing the echo decay with increasing pulse separation and T_1 by watching it recover from r.f. saturation, i.e. microscopic randomization of M in all directions.

Consider using these three methods to check the validity of the screening model. For example, it is possible that the Cu impurity might possess a small moment, due to the available s and d electrons not being able to screen the Cu in as short a distance as is conceivable, i.e. an extended disturbance. The diffuse neutron scattering is proportional to the difference in the moments of the impurity and the host. It is already difficult to measure a difference as small as 0.6 μ_B, as in the case of the screening model. Distinguishing the case of no moment on the Cu from one with 0.1-0.2 μ_B would be very difficult. The problem with the n.m.r. or Mössbauer measurement of the hyperfine field is in interpreting the results. The origin of the hyperfine is not well

enough understood to allow one to draw conclusions about the impurity moment from the measured hyperfine field. That is, the estimates of the contributions of the different possible effects to the hyperfine field on an impurity in a ferromagnet are not good enough to deduce the impurity moment.[9] Similarly, the measured difference in H_n of atoms which are nearest neighbors to an impurity doesn't imply a particular difference in moment because of the unknown magnitude of this and other effects. (If one could deduce the change of moment of the nearest neighbor Ni's, one would know the Cu moment from the observed average decrease of 1 μ_B/Cu atom.)

It will be shown in section II B that measurement of the Cu longitudinal relaxation, interpreted according to Moriya's theory of relaxation in ferromagnetic transition metals[10] gives clear evidence in favor of the screening model, that is, a very small or zero moment on an isolated Cu impurity in Ni. Thus, measurement of nuclear relaxation of the impurity gives the clearest picture of the electronic behavior in the vicinity of the impurity in this particularly simple case.

Chapter I

DYNAMICS OF THE RESONANCE

The nuclear magnetic resonance excitation and resulting signal are enhanced in a ferromagnet due to the mediation of the electronic magnetization between the nuclei and the apparatus.[5] In the presence of domain walls the signal is dominated by nuclei in the walls. This is because the walls move to shield the domain bulk, which does not feel the r f excitation, as well as because the walls have a much larger enhancement factor than the bulk.

Consider the idealized case of a spherical particle with a single 180° wall in the middle (Fig. 3a). If a field is applied in the x-direction, the wall moves to minimize the sum of the demagnetizing energy and the interaction energy of the non-zero magnetic moment of the sphere with the external field. For small fields, the displacement of the wall Δz is:[5, 11]

$$\Delta z/d = (1/4\pi)\, H_x/M \qquad \text{I-1}$$

The demagnetizing field created by the sphere's induced moment just cancels the external field. Thus the domain bulk is shielded by the walls.

Now consider a nucleus in the wall which feels a hyperfine field H_n antiparallel to the local direction of magnetization. When the wall moves, M rotates to a new angle θ with respect to the direction of magnetization in the bulk. H_n at the nucleus follows M, giving rise to a transverse field, H_{eff}.

$$H_{eff} = H_n\, \Delta\theta = H_n \frac{\Delta\theta}{\Delta z}\, \Delta z = \frac{H_n}{4\pi M_s}\, d\, \frac{d\theta}{dz} = \eta H_x, \qquad \text{I-2}$$

where η is the enhancement factor.

The theoretical curve of θ versus z[12] is shown in Fig. 3b. Near the center, it can be approximated by a uniform rotation:

$$\frac{d\theta}{dz} = \frac{\pi}{\delta}, \qquad \text{I-3}$$

which gives $\eta = \frac{H_n}{4M_s}\frac{d}{\delta}$. Cowan and Anderson[13] have measured this enhancement in pure Ni using the rotary saturation technique. They find $\eta = 1700$ experimentally. They find $\eta = 2000$ for Fe, which is consistent with Eq. I-2 as the ratios $\frac{H_n}{M_s}$ and $d\frac{d\theta}{dz}$ are nearly equal for Fe and Ni. As seen in Fig. 3b, the wall trails off gradually, with $\frac{d\theta}{dz}$ decreasing to zero. Therefore the nuclei in the wings of the wall feel a smaller enhancement than those in the center.

In a single domain particle (or saturated multidomain particle), the enhancement comes about by domain rotation. This rotation is impeded by a field H_a, which comes from magnetocrystalline anisotropy and the externally applied field, H_o. In the absence of a perturbing field, M is along H_a, as shown in Fig. 4. H_x, applied perpendicular to H_z, tips M by an angle $\theta = H_x/H_a$, for small H_x. This produces an effective transverse field:

$$H_{eff} = \theta H_n = \frac{H_n}{H_a} H_x = \eta H_x \qquad \text{I-4}$$

In the case of Ni, $H_n = 75$ kG and $H_a = 2$ kG, giving $\eta \simeq 40$, which is much less than the enhancement of 1700 at the center of the walls.

In this study, I have sought to measure the relaxation rates of nuclei in the domain bulk. The nuclei in the wall can relax by mechanisms peculiar to the wall.[14,15] These mechanisms usually dominate the wall relaxation, which is thus considerably faster than the bulk relaxation. The domain relaxation, caused by the

fluctuations of the magnetic interactions, is of more general interest than the special properties of domain walls. It is also more amenable to ab initio calculation of the various relaxation mechanisms. There is fairly good agreement between Moriya's[10] calculations and the measured longitudinal relaxation times in the pure ferromagnetic metals: Co, Fe, and Ni. This makes it desirable to measure the relaxation in the simple alloy, Ni-Cu, in the domain bulk.

Although relaxation times can be measured by c w methods[16, 17] it is much easier using transient means.[8] This method allows a direct measurement of the transverse and longitudinal relaxation times, as well as facilitating the separation of the wall and bulk signals. This can be done in one of several ways. As pointed out above, the enhancement factor decreases away from the center of the wall. If one applies an intense r f pulse, H_1 greater than 10 Oe, the spins in the center of the wall are driven through many rotations, while in the wings of the walls, the rotation angle goes continuously to zero. The signals from the center of the wall tend to average out as small changes in conditions leave the spins pointing in very different directions, while spins with enhancement factors such that $\theta = \eta\gamma_n H_1 t_w \simeq \pi/2$ are under optimum echo conditions. Here η is the enhancement factor, γ_n the nuclear gyromagnetic ratio, $2H_1$ the applied r f field (H_1 is the amplitude of one circularly polarized component), and t_w the length of the pulse. Thus, the larger the r f field, the more contribution to the signal from spins with lower enhancement, i.e. further out in the tail of the wall.[14] Although the high enhancement spins' signal is

reduced by this cancelation, nonetheless this signal is predominant at short pulse separations. However, as mentioned above, the wall relaxation is dominated by mechanisms peculiar to the wall. These mechanisms decrease in effectiveness as one goes out in the wall. Thus, the strong, center-wall signal decays fast and one expects a slower relaxing signal at long times. This behavior has been observed and is shown in Fig. 6. One might expect that far enough out in the wall, the relaxation would be dominated by bulk processes, and one would observe the signal approach a straight line, corresponding to a constant relaxation rate. Weger claimed to observe this in his experiments on Co, Fe, and Ni. He gave these long time relaxation rates as the "bulk" values.[11, 15] Thus, by using high power pulses and using the rates observed at the longest times, one measures relaxation in the wings of the wall, which may approach bulk relaxation.

Another method of measuring bulk relaxation is to apply a d c magnetic field pulse during the time in which the spins are relaxing. In this way one uses the walls as enhancers of the exciting r f and the detected signal, but moves the walls with the field pulse during the relaxing time. The walls are moved far enough so that the nuclei reside in the bulk and relax according to bulk processes. This method was used by Kaplan, Jaccarino and Wernick,[19] who found good agreement between relaxation rates of Mn^{55} in Fe measured this way and by the high power method described above.

Finally, one can apply a large steady magnetic field to drive out the walls and saturate the magnetization along the direction

of the field. In the absence of walls, the enhancement is by domain rotation and one sees a true domain bulk signal. Of course, this value is not necessarily identical with the zero-field bulk relaxation rate, because of the field dependence of the relaxation.

The walls are driven out when the external field exceeds the demagnetizing field, NM. For a sphere $N = 4\pi/3$. For Ni (or Ni with a small amount of Cu) M (0°K) = 510 G. Therefore the domain structure is energetically unfavorable for a field greater than 2.1 kG. However, due to crystal imperfections which act to impede the wall motion, it is possible for walls to continue to be present to higher fields than the demagnetizing field. One could ignore these pinned walls if the r. f. field is applied parallel to the saturating field. With the walls pushed hard against the pinning center, a weak r. f. field acting in the same direction would not significantly move the walls. However, compared to the configuration of Fig. 4, a much smaller enhancement results for H_x parallel to H_o, because the r f field H_x cannot tip M, except to the extent that M is canted from the parallel direction by an internal anisotropy field. No signal was observed using this configuration for Cu in Ni in a large d c field.

In the perpendicular field case, it is conceivable that the pinned walls would be free to move in response to H_x. However, it seems unlikely that these pinned walls would be very mobile. Therefore, they would not experience much enhancement or be able to shield the rest of the particle from the r f field. The Cu^{63} echo signal for 2% Cu in Ni was observed in high field, 4 to 8 kG, in the perpendicular configuration. The echo maximum was sought as

a function of r. f. pulse width for the maximum r. f. power. This was measured by observing the voltage in a pickup coil tightly coupled to the sample coil. The value of the field at the end of the coil is perhaps half of that in the center. The measured value of H_1 was 14 G. In an external field of 6 kG, the signal was maximum for both r. f. pulses 2μs long. The enhancement factor is $H_n/H_o \simeq 47/6 = 7.8$. Therefore the turning angle for spins in the saturated domains is:

$$\theta = \eta\gamma_n H_1 t_w = (7.8)\ (7.0 \times 10^3)\ (14)\ (2 \times 10^{-6}) = 1.5 \text{ radians or } 86° \qquad \text{I-5}$$

With the possible upward variation in H_1 over the sample, this indicates a turning angle of 90° - 180° for spins in the bulk enhanced by domain rotation. The fact that the signal maximizes in this region indicates that these spins are responsible for the high field resonance.

The isolation of the domain signal can be further investigated by measuring the nuclear resonance frequency as a function of externally applied field. Portis and Gossard[5] observed that the Co^{59} resonant frequency decreased very little in a field up to 5 kG, while the signal strength had decreased by a factor of 100. This is evidence that the signal originates in the domain walls. In an external field the walls move so as to create a demagnetizing field which very nearly cancels the external field. The reduction in signal is due to the driving out of the walls at fields equal to NM, where N is the demagnetizing field. Measurements of the resonant frequency of Ni^{61} in Johnson-Matthey 99.999% Ni sponge are shown in Fig. 5.

The signals were measured with $H_1 \simeq 0.5$ G and pulse widths which gave a maximum echo in zero field. The r f frequency and apparatus tuning were adjusted with field for maximum signal. The frequency of the echo was measured by beating it with a weak c w signal. The frequency starts flat as expected for wall signals. It begins to bend significantly by 2 kG. The Johnson-Matthey sponge particles were observed under a microscope to be roughly spherical, that is all dimensions about the same, with a diameter of 5 - 10μ. For a sphere, the coercive field is $(4\pi/3)$ M = 2.1 kG. The signal decreases in strength as the walls are driven out, until the signal is dominated by the unshielded domain signal, which is weaker because of the smaller enhancement. In the saturated regime, one must consider the anisotropy field, H_a.[20] Since the crystals in the powder are randomly distributed, the particle magnetization will align along the resultant of H_o and the internal H_a. So only for $H_o >> H_a$ will the sample be fully magnetized along H_o. In Ni at helium temperature where these frequency data were taken, $K_1 = -7.5 \times 10^5$ erg/cm^3.[21] For small deviations from the easy [111] direction, $H_a = -4K_1/3M = 2.0$ kG. If H_o is at some angle to H_a, the process of magnetizing the particle along H_o is opposed by the demagnetizing field plus the projection of H_a along H_o. In the most unfavorable case, this will be the full internal H_a. Therefore, we expect the sample to be mostly magnetized for $H_o \geq H_a + NM \simeq 4$kG for spherical Ni particles. As shown in Fig. 5, the frequency is linear with H_o

above about 4 kG, in agreement with this argument.

In fields $H_o >> H_a$, the domains are fully magnetized along H_o and the nuclei feel the hyperfine field plus the local field. As usual, the local field consists of the external field plus demagnetizing fields from the surface of the spherical particle, the surface of the imaginary spherical cavity in which the particle sits, and the outer surfaces of the sample. Because the sample is a powder, the magnetization in the sample is reduced by the filling factor f.

Therefore:

$$H_{loc} = H_o - \frac{4\pi}{3} M + \frac{4\pi}{3} fM - NfM = H_o - \frac{4\pi}{3} M(1-f) - NMf \qquad I-6$$

The Ni sponge used has f = 0.35. The sample is cylindrical with a length to diameter ratio of 1.5. The field is applied perpendicular to the axis of the cylinder. For this geometry the demagnetizing factor along the axis is roughly $4\pi \times 0.18$,[22] giving a demagnetizing factor perpendicular, $N = 4\pi \times 0.41$.

Therefore at high fields, the field at the nucleus is $-H_n = -H_{no} + H_{loc}$, where the hyperfine field is indicated negative, as it is in the opposite direction from $\underline{M}$.

$$H_n = H_{no} + \frac{4\pi}{3} M (1-f) + NMf - H_o = H_{no} + 2.3\,kG - H_o \qquad I-7$$

The domain wall resonance at zero applied field measures H_{no} since the spins in the center of the wall are perpendicular to the magnetization. Thus, in the absence of H_o and demagnetizing fields, the zero field resonance frequency is $(\gamma_n/2\pi)\, H_{no}$. The dotted line has a slope appropriate to Ni^{61}, $\gamma_n/2\pi = 0.38$ Mc/kG. The $H_o = 0$ intercept predicted by Eq. I-7 is designated by the ▲ in Fig. 5.

The field dependence of the Cu^{63} resonance in a 2% Ni-Cu alloy is more complicated and is shown in Fig. 6. At low external fields, 0 to 2 kG, a strong signal is observed with weak r f pulses. In intermediate fields, 2 to 4 kG, a wide band of signal frequencies is observed with the higher frequencies stronger at lower power and the lower frequencies at high power. When the higher frequency signals are excited with high r f power, the echo has a sharp maximum for $t_{w1} = t_{w2}$, indicating that this signal is from high enhancement spins which are driven through a rotation of many revolutions. When the two turning angles are equal, all the various enhancement contributions add coherently, but when the pulses differ slightly, the turning angles differ by a half revolution or more and the different contributions add with random phases and cancel. At fields above 4 kG, only the low-frequency, high-power signal is observed.

The low-field signal originates in the higher enhancement domain walls as indicated by its excitation at low powers. The intermediate region is due to coexistence of saturated particles with particles still containing domain walls. The Ni-Cu alloy samples were ground from a rod using bonded abrasive paper containing 120 mesh Al_2O_3 particles. The sample particles were observed to be worm shaped with diameters in the range 10-25 μ and lengths 1 to 30 times the diameter. With this shape particle, there is no single demagnetizing factor, and there is an intermediate frequency range, in which saturated particles and particles with walls coexist. The coercive field for short worms is about like that of a sphere, $(4\pi/3)M$. For long worms, it varies from zero for magnetization along the axis, of which there will be few because of the small solid

angle in this direction, to $2\pi M$ in the direction perpendicular to the axis. Therefore one expects coexistence of significant populations from somewhat below $4\pi/3M$ to somewhat above $2\pi M$, or 2.1 to 3.2 kG.

The possibility was considered that the echoes observed in the intermediate region at high power might be high-frequency wall signals excited by the sidebands of the square r f puse which are spread out in multiples of $1/t_w$ in frequency. These sidebands are weaker, which would be advantageous for exciting high-enhancement wall signals. It would also explain the critical dependence on $t_{w1} = t_{w2}$ as only in this condition do the sidebands of the two pulses coincide. However, this possibility is eliminated because the measured frequency is that of the echo. If the above explanation held, the echo signal would be at the free precession frequency, and not the central frequency of the oscillator.

In the high field region, the frequency of the domain signal does not decrease linearly with external field, although it does seem to approach the correct slope asymptotically as shown in Fig. 6. As mentioned in connection with the Ni signal, the particles are not fully saturated until $H_o >> H_a$. Bozorth[21] tabulates anisotropy data for Ni-Cu alloys, giving a value for 2% Cu at 0°K, $K_1 = -6.9 \times 10^5$ erg/cm^3. This gives $H_a = -4K/3M = 1.8$ kG. However, in Fig. 6, one sees appreciable curvature in the frequency up to about 10 kG. This extra apparent anisotropy may be due to strains or inhomogeneity of the alloy.

As with the Ni^{61} resonance, we take the zero field resonance

as corresponding to a field H_{no}. We compare the high-field linear field dependence region extrapolated to zero field minus H_{no} with the calculated demagnetizing field. In calculating the demagnetizing field due to the individual particles, there is no unique demagnetizing factor as discussed in connection with the coercive field. For nearly spherical particles, $N \simeq 4\pi/3$. In the long worms, N varies from zero to 2π with an average closer to the latter because of solid angle. For an estimate of the effect we use $N = 4\pi/3$. The density of the Ni-Cu sample gives $f = 0.30$. The sample geometry is the same as the Ni sponge. Using Eq. I-7, there is a demagnetizing field $(4\pi M/3) \times 1.13 = 2.4$ kG. This difference is indicated by the ▲ in Fig. 6.

Thus the observed resonances in Ni^{61} in Ni and Cu^{63} in Ni-Cu have been determined to originate in spins in the domain wall (perhaps well out into the tail of the wall with high power r.f. pulses) in low external field and in the saturated domain bulk in high external field. In the alloys, there is intermediate field region in which the two types of signals coexist.

Chapter II

LONGITUDINAL RELAXATION

A. Experiment

The longitudinal relaxation time, T_1, can be measured in two ways. The more straightforward is the saturation method. This involves using the ordinary spin echo to monitor the recovery of the z-magnetization following saturation of the magnetization by a series of r.f. pulses, called an r.f. "comb". The other is the stimulated echo,[8] which is observed a time τ after an r.f. pulse, which follows a pair of r.f. pulses separated by τ, setting up a modulation of the z-magnetization. Since this modulation washes out in a time T_1, in the absence of diffusion, the stimulated echo decays in a time T_1.

The stimulated echo is experimentally simpler. Even though the stimulated echo is weaker than the ordinary echo, it gives a better signal-to-noise ratio. This is because in the saturation method at long times, one must accurately measure small increments on a largely recovered signal, whereas the stimulated echo is proportional to the undecayed z-magnetization, so one can follow this portion further down into the noise.

The saturation method, however, is more certain of interpretation. If one is convinced saturation is achieved,[23] one has measured the time for longitudinal relaxation, T_1, directly. The formation of the stimulated echo is more complicated, involving the value of T_2, if diffusion effects are appreciable. In this case one observes an additional term in the relaxation rate proportional to τ^2.

Measurements of the T_1 of Ni were made in pure Ni

sponge and in the 2% Ni-Cu sample, using both methods to compare the results. The relaxation rate of the stimulated echo, for small τ is given by:[11]

$$\frac{1}{T_{se}} = \frac{1}{T_1} + 4\pi D_\nu \tau^2 \qquad \text{II-1}$$

where D_ν is the constant for diffusion in frequency. A small, roughly linear dependence on τ^2 of the stimulated echo of Ni^{61} in Ni sponge and Cu^{63} in the 2% alloy has been observed. For comparison of the stimulated echo and saturation methods, τ was made small enough so that the second term in II-1 is less than 1% of the first. This is well within experimental error, so the relaxation time measured can be considered the stimulated echo value of T_1.

Since the high-field relaxation rate is the one governed by intrinsic domain processes,[24] the T_1 by stimulated echo and saturation were measured as a function of field. In a small external field, the observed relaxation is non-exponential, showing a decreasing relaxation rate for short times. This behavior was explained in Chapter I. The exponential signal at long times corresponds to spins far out in the domain walls, which feel little fluctuation from the wall motions and thus relax slowest.[2] It is this limiting value which is taken as the "bulk" relaxation rate. Fig. 7 presents data for the longitudinal relaxation by the stimulated echo method of the Cu^{63} resonance in zero field, showing the behavior just described.

A comparison of the T_1's measured for Ni^{61} in pure Ni sponge are shown in Fig. 8. These data were taken at moderate r.f. levels,

$H_1 \simeq 3G$. Saturation was achieved by applying a series of long r f pulses, typically 20 pulses of width five times the echo-producing pulses. In order to saturate the whole resonance line, one needs sufficient r f power to significantly tip all the spins in the line away from the z-axis, viewed in the rotating frame. This condition is:

$$H_{1,eff} >> \frac{\Delta\omega}{\gamma_n} \qquad \text{II-2}$$

The linewidth for Ni^{61} in pure Ni is about 150 kHz at 4.2°K. This was measured directly by sweeping the frequency of large width r. f. pulses and taking the full width at half height of the echo. The width of the pulses is made large to assure that the frequency distribution of the r f pulse is narrow compared to the linewidth. It was also measured by observing the width, T^*_2, of the echo following short, high power pulses which excite the whole line. This is converted into the linewidth by the fact that $\Delta\omega \propto \frac{1}{T_2^*}$. The two methods agree within the measured accuracy of about 25%. With this linewidth the condition, II-2 becomes $H_{1,\,eff} >> 400G$. For the wall signal, we expect $\eta \simeq 100\text{-}1000$ depending on how far out in the wall we look. For $H_1 = 3G$, we get:

$$H_{1,\,eff} = \eta H_1 = 300\text{-}3000G. \qquad \text{II-3}$$

Thus, the condition II-2 is at worst barely fulfilled. We expect that with a train of many long r f pulses, most of the line will be rotated from the z-axis. Because of the random phases of the successive saturating pulses, the various magnetization components will undergo a series of random angular displacements, ending up in the saturated state, that is, one with nuclear spins pointing randomly in space. Therefore, there is no ordinary echo signal until some of the magnetization has relaxed back to the z-axis, so the echo following saturation measures the

longitudinal relaxation.

Comparing the $1/T_1$ values of Fig. 8a) and b), we see that the two methods give fair agreement for H = 0, with the saturation method showing somewhat slower relaxation than the stimulated echo. However, on applying a static field large enough to saturate the domains, we see that the relaxation rate by the stimulated echo method stays essentially constant, while that by saturation shows a significant decrease. Since we are trying to discriminate the longer, "bulk", relaxation time, preference should be given to the method measuring longer relaxation times. That is, it is possible to imagine additional, non-intrinsic mechanisms increasing the stimulated echo relaxation rate, but since the various relaxation rates are additive, the smaller saturation rate must be considered an upper limit on the high-field domain relaxation rate. The objection that in the high-field, domain region, with its lower enhancement, saturation may not be achieved does not apply because in the event of incomplete saturation, there will be a faster apparent relaxation, as the excited nuclei relax by diffusion into unexcited ones.[23] Therefore, the above statement about an upper bound on the intrinsic relaxation rate holds. Finally, the dependence of the relaxation rate on field as measured by saturation agrees well with that measured by Jaccarino et al.[24,25] This dependence is shown asymptotically by the lines in Fig. 8 a). For these reasons, the saturation method is preferable for measuring T_1, particularly in the high field region.

Similar behavior of the Ni^{61} resonance in the 2% Ni-Cu alloy was observed using the two methods. The stimulated echo rate is larger

and roughly constant as a function of field. The high-field, 3kG and higher, values of the relaxation measured by saturation agree with those in pure Ni, i.e. at 4.2°K, $T_{1,H\geq 3kG} \simeq 35$ ms.

The longitudinal relaxation data previously reported[26] for Cu^{63} in a 2% Ni-Cu sample was measured in zero external field, using the stimulated echo technique at four temperatures: 2.1°K, 4.2°K, 77°K and 300°K. The T_1 was taken from the long time exponential part of the curve, as shown in Fig. 7. The near equality of zero field relaxation rates found by the two methods for Ni^{61} indicates that these T_1's measured by stimulated echo can be taken as the zero field "bulk" value. The T_1's are in fair agreement with a relation T_1T = const. as shown in Fig. 9. The signal-to-noise ratio is better at low temperature, so the 45° line is heavily weighted to these data, giving a value $(T_{1,\ H=0}T)^{-1} = 10\ \text{sec}^{-1}\text{K}^{-1}$.

Longitudinal relaxation of Cu^{63} in the high field region has been measured in four dilute alloys: 1, 2, 2.5, 5% Cu in Ni at temperatures: 2.1°K, 4.2°K, and 77°K. The high-field, domain signal was much weaker than the zero-field, wall signal, due to the low enhancement. Therefore, the relaxation was measured at 77°K only in the 5% alloy, where the signal was strong enough to get accurate values, to check the temperature dependence over a wider range than a factor of two.

The high-field domain relaxation is exponential, as can be seen in Fig. 10. The straight line fitting the data does not extrapolate to zero signal at t = 0, i.e. immediately after saturation. This indicates possible incomplete saturation, resulting in fast apparent relaxation as the incomplete saturation diffuses through the whole line, and then slower, intrinsic relaxation as the remaining magnetization

relaxes to the z-axis. The diffusion takes place in a time of the order of the spin-spin time, which we will see in the next Chapter is of the order of 10-20 ms. The data shown in Fig. 10 deviate upward from the straight line up to about 50 ms. We again calculate, for the high-field Cu^{63} data, to what extent the saturation condition, (II-2), is satisfied. The linewidth of the Cu^{63} resonance at 2.1°K and 4.2°K in the 2% Cu sample was found to be about 350 kHz, estimating from the observed width of the echo excited by narrow r.f. pulses. As in Chapter I, η = 47 kG/6 kG = 7.8. H_1 = 14 G. Then:

$$H_{1,eff} = \eta H_1 = 110 \text{ G} < 320 \text{ G} = \Delta\omega/\gamma_n \qquad \text{II-4}$$

The saturation condition goes the wrong way and we expect effects of incomplete saturation. The fact that the straight portion extrapolates to $1-M/M_o = 0.75$ indicates that the line is roughly 75% saturated. This means that 75% of the spins coupled to the spins involved in the observed signal are sufficiently tipped away from z-axis and randomized by the r.f. comb to be considered saturated.

The relaxation rate for a particular alloy at a particular temperature is quite constant as a function of field in the high field region as defined in Fig. 6. There is a barely significant tendency for T_1 to increase for higher field. This is indicated for the four alloys at different temperatures in Fig. 11. When T_1 was measured in the intermediate field region, it was found that if the echo was excited at the low frequency end of the intermediate band shown in Fig. 6, the value of T_1 lined up well with the high field value. If the echo corresponded to a middle or high frequency in the intermediate region, the value of T_1 ranged down from the high field value to a considerably smaller

value, though never as small as the zero field T_1. This is shown in Fig. 11 b) where the low frequency resonance is labelled (l) and the high frequency one (h). In more extreme cases, the high-frequency time was a factor of three shorter than the low frequency one. This is in agreement with the interpretation suggested in Chapter I, that the low-frequency signal comes from fully saturated particles, while the high-frequency one comes from particles with a higher coercive field, thus containing domain walls.

The field dependence of T_1 in the high field region and the low frequency part of the intermediate field region is so slight that a mean value of T_1 appropriate to the 6-8 kG region can be taken as the high field domain bulk longitudinal relaxation time. This value is indicated by the dotted lines in Fig. 11. Similarly constant high field relaxation rates were reported in Refs. 24 and 27. The high-field relaxation rates, with a factor of temperature taken out, are shown in Fig. 12 as a function of Cu concentration. The error bars represent the combined uncertainty due to scatter of the data about pure exponential relaxation and uncertainty in determining the high-field value of T_1 from the measured values in the range 6-8 kG. The large error in the 2%, 4.2°K value arises from the fact that this was the first large-field, high-power data taken, for which such slow relaxation was not expected. Hence, the signal was not meausred far enough out in time and an accurate measure of the signal strength at long times was not obtained. The error for the 5%, 77°K run reflects the poorer signal-to-noise ratio at this high temperature, inducing more scatter in the data.

The data obeys the relation T_1T = const. for each concentration within the indicated error. It is not understood why the 2% sample has the higher relaxation rate shown in Fig. 12. All four samples were ground identically with Al_2O_3 abrasive paper and strain annealed in a vacuum of about 10^{-4} mm of Hg at 600°C for a half hour. The 2.5% and 5% Cu samples were prepared by the Materials Research Corp., while the 1% and 2% alloys were melted from the powder in a 4% H_2, 96% He reducing atmosphere, cooled as quickly as the furnace would allow, and raised to a temperature about 30°C below the melting point for a day to homogenize them by diffusion. It is hard to see how inhomogeneity would raise the relaxation rate as it is very nearly independent of concentration.

With no clear dependence on concentration and no reason for expecting anomalous behavior for the 2% Cu sample, we must conclude that the measured relaxation rate is independent of concentration up to 5% Cu. The mean value of this rate and r.m.s. deviation are determined by weighing the data in inverse proportion to the estimated error. This gives a value of $1/T_1T$ equal to $(0.98 \pm .10)$ $sec^{-1}{}^{\circ}K^{-1}$. This value and limits of error are shown by the horizontal lines in Fig. 12.

B. Comparison with Theory

Moriya[10] has calculated the expected longitudinal relaxation rate in the ferromagnetic transition metals Fe, Co, and Ni. He concludes that the primary contribution to the relaxation is thermal fluctuations of the orbital field at the nucleus produced by the d band electrons, which are treated in the tight binding approximation.[28] Korringa relaxation by the 4s conduction electrons via the Fermi contact interaction is sometimes appreciable, while other mechanisms, such as dipolar and

spin wave related mechanisms, were found to be negligible. Since both orbital and Korringa rates, as direct processes, are proportional to the absolute temperature as well as the square of nuclear coupling, γ_n, it is convenient to consider the relaxation rate in the form $(\gamma_n^2 T_1 T)^{-1}$, which shall be designated R. This expression, which is proportional to the square of the thermally fluctuating field at the nucleus, facilitates comparison of the relaxation rates in different materials.

After account is taken for the mistakes in the original paper, involving the densities of states, Moriya calculated for the orbital relaxation in Ni:[10] $R_{d\ orb.}^{Ni} = 8 \times 10^{-7}$. The value of the s contact relaxation in Ni estimated from the known values for Cu and again corrected for the mistake in the density of states, is $R^{Ni}_{s\ contact} = 0.2 \times 10^{-7}$. The experimental values for Ni are $R^{Ni}_{H=0} = 15 \times 10^{-7}$, $R^{Ni}_{high\text{-}H} = 10 \times 10^{-7}$.[25] Thus, in Ni, the s contact mechanism is negligible in comparison to the d orbital relaxation. The high-field relaxation rate, which, it has been argued, is the intrinsic domain rate appropriate to the calculation, is in agreement with the calculated d orbital rate within the accuracy of the estimate, indicated by Moriya, of about 50%. Thus the high-field relaxation in Ni can be considered satisfactorally understood.

The experimental rates for dilute Cu in Ni, given in IIA, are $R^{Cu}_{H=0} = 2.0 \times 10^{-7}$, $R^{Cu}_{high\ H} = (0.19 \pm 0.02) \times 10^{-7}$. The excess relaxation rate for zero field over that at high field is attributed to a mechanism related to the domain walls, whose thermal motion relaxes the nuclei in the wings of the walls, where the high-power, long-time signal originates in zero field. For Cu in Ni, this wall rate is about

1.8×10^{-7} while for Ni in Ni it is 5×10^{-7}. Since R is proportional to the square of the fluctuating field at the nucleus and motion of the wall is involved, it is reasonable to take this field to be proportional to the total field at the nucleus, H_n. These hyperfine fields are 75 kG for Ni in Ni and 47 kG for Cu in Ni.[29] So we would expect: $R_{wall}^{Cu} / R_{wall}^{Ni} = (H_n^{Cu}/H_n^{Ni})^2 = 0.39$. This agrees remarkably with the ratio of the experimental values, 0.36. This numerology is merely suggestive, since the actual wall mechanism hasn't been specified or worked out.

More importantly, we notice that the high-field Cu in Ni relaxation rate is of the order of the estimate of the s contact relaxation rate in Ni. In order to examine the possible agreement with experiment, we consider the situation for Cu in Cu. There is substantial disagreement among the experimental determinations, all of which were made by observing the onset of saturation in a c.w. experiment as a function of the r.f. field, H_1. These are shown in Table 1. One problem is that at low H_1, one may not excite the whole resonance line and thus measure apparently faster relaxation due to diffusion into the rest of the line, as previously mentioned.[23] The high power, transient method gives the most reliable measure of the relaxation, but none is available for Cu. It is reasonable to eliminate the first entry in Table 1 because of its deviation from theory and the other experiments on the fast side, possibly due to incomplete saturation.

The Fermi contact relaxation rate is given by:

$$(\gamma_n^2 T_1 T)^{-1} = \pi k_B \hbar^3 \gamma_e^2 \left(\frac{16\pi}{3}\right)^2 \langle|\psi(0)|^2\rangle_{FS}^2 [\rho(\epsilon_F)]^2 \quad [34] \qquad \text{II-5}$$

where $\langle|\psi(0)|^2\rangle_{FS}$ is an average over the Fermi surface and $\rho(\varepsilon_F)$ is the density of states at the Fermi surface of both directions of 4s spins. Since the same interaction is responsible for the s contact relaxation and the Knight shift in metals, they are closely related, in the nearly free electron model, in which the denisty of states (relaxation) is proportional to the susceptibility (Knight shift). This is the Korringa relation:[35]

$$(\gamma_n^2 T_1 T)\ (\Delta H/H)^2 = \hbar\gamma_e^2/4\pi k_B \qquad \text{II-6}$$

Pines[36] has considered the effect of the electron-electron interaction, which affects the density of states and the susceptibility differently. He determined the ratio of the density of states with electron-electron interactions from the experimental low temperature specific heat, which of course reflects these interactions. He calculated how the susceptibility is changed, using many body theory. Using these, he obtained a modified Korringa relation. These are tabulated in Table 2.

The mean experimental relaxation rate is between the theoretical ones, being closer to and larger than Pines' collective result. This errs in the right difection, as there may be other mechanisms unaccounted for. So within the 20% error in the experiment, the relaxation rate in Cu is accounted for by s contact Korringa relaxation.

In order to estimate the expected relaxation rate for Cu in Ni, one must consider the d orbital and s contact mechanisms. With a naive interpretation of the rigid band model, one might expect the densities of states appropriate to these rates to be the Ni densities of states at a higher ε_F, corresponding to the higher electron concentration. Since $N_d(\varepsilon)$ is not smooth, but varies rapidly in energy,

the possibility that the small rate for Cu in Ni reflects a dip in $N_d(\varepsilon_F)$, which minimizes the d orbital contribution, must be considered. That this is not the case is indicated by the lack of concentration dependence of the relaxation shown in Fig. 12. $N_d(\varepsilon_F)$ is large in pure Ni, and it seems unlikely that it would drop abruptly with 1% Cu and stay there up to 5% Cu. A more conclusive argument is that the Ni relaxation rate was measured in high field in the 2% Cu alloy and was found to be close to the pure Ni high field value. This indicates a considerable d density at the Ni sites in the alloy.

The observed Ni signal is believed to come from Ni's which are not nearest neighbors to the Cu impurity. In an f.c.c. lattice, with 2% Cu impurities, these Ni's constitute about 4/5 of the total. In the screening picture of Fig. 2, these Ni's are outside the range of the effects of screening the Cu. Thus, it is consistent with this model that the Ni relaxation rate in the alloy be nearly the same as in pure Ni.

In the screening model, it is assumed that the d states of the isolated Cu are filled. There is no possibility of a d orbital relaxation mechanism, involving fluctuations of the orbital field at the nucleus, as all the states are continually filled. Thus the screening model allows only s contact relaxation. We can estimate this from the value for Cu in Cu. It is assumed that the average density of an s band electron at the Cu nucleus is the same in the alloy as in pure Cu. Then, it is only necessary to compare the s densities of states to calculate the relaxation rate from II-5. The s band can be treated in the nearly free electron approximation for which $N_s(\varepsilon_F) \propto \frac{n}{\varepsilon_F} \propto n^{1/3}$, where n is the number of s electrons/unit volume. For the isolated Cu in Ni, there are

0.54 electrons of pure Ni plus 0.1 electron in the screening cloud. In Cu there is one 4s electron/atom. So for the screening model we expect:

$$\frac{1/T_1)^{\text{Cu in Ni}}}{1/T_1)^{\text{Cu in Cu}}} = \left[\frac{N_s(\epsilon_F)^{\text{Cu in Ni}}}{N_s(\epsilon_F)^{\text{Cu in Cu}}}\right]^2 = (0.64)^{2/3} = 0.74 \qquad \text{II-7}$$

Taking the mean experimental value for Cu in Cu, which was in agreement with theory, and the value measured in the present work, we find the experimetal ratio:

$$\frac{(\gamma_n{}^2 T_1 T)^{-1}\ \text{Cu in Ni}}{(\gamma_n{}^2 T_1 T)^{-1}\ \text{Cu in Cu}} = \frac{0.19 \pm .02}{0.20 \pm .04} = 0.95 \pm .3 \qquad \text{II-8}$$

The screening model prediction falls within the experimental error. However, if it is assumed that the estimated error is too conservative, comparison of II-7 and II-8 shows that the Cu in Ni relation is slightly faster than expected from Cu in Cu. This excess relaxation is of the order $(\gamma_n{}^2 T_1 T)^{-1}_{\text{excess}} \times 10^7 \simeq 0.05$. When this is compared to $(\gamma_n{}^2 T_1 T)^{-1}_{\text{d orbital}} \times 10^7 = 8$, it is clear that there is very little, if any, d orbital contribution to the relaxation.

Of course, the explanation of the relaxation rate presented here is vastly oversimplified. The screening model is a localized picture, whereas the density of states is a band concept, whose applicability has not been shown. Furthermore, the interactions between an impurity and adjacent host atoms are more complicated than the screening picture, specified only by electron populations, indicates, including effects on more distant neighbors. The interpretation of the data rests on the observation that the relaxation rate measured for Cu in Ni is nearly the same as for pure Cu, which, in turn, is in close agreement with a calculation based on the Fermi contact interaction. In view of

the large contribution of d orbital fluctuations in Ni compared to the s contact rate, this agreement indicates that little part is played by d fluctuations. This, in turn, indicates that there are few, or no, d holes on the Cu impurity, i.e. little or no moment, as one would expect the high density d electrons in Ni to scatter strongly with any Cu moment, thereby adding to the relaxation rate. The screening model provides a simple physical picture of the behavior around a Cu impurity in Ni, reflecting these conclusions.

Chapter III

TRANSVERSE RELAXATION

A. Experiment

The transverse relaxation time, T_2, is measured by observing the decrease of the spin echo amplitude as the spearation of the echo producing pulses, τ, is increased. The first pulse tips the nuclear magnetization from the z-axis, creating a coherent transverse magnetization, which quickly disappears due to inhomogeneous broadening. The second pulse again rotates the nuclear magnetization and reorients the previous transverse magnetization to a position where it proceeds to "unwind" the reversible decoherence, producing the echo an equal time later. During this time, interactions of the nuclear spins, with each other or with the lattice have been producing an irreversible dephasing of the transverse magnetization, which reduces the echo at 2τ. This relaxation process can be characterized by a single parameter, T_2, only if the echo amplitude obeys the relation:

$$A(t) = A_0 e^{-2\tau/T_2} \qquad \text{III-1}$$

This exponential behavior corresponds, by Fourier transform, to a Lorentzian shape for the homogeneous line. If the line is Gaussian, so will the relaxation be. It is then customary to characterize the relaxation by the time for the echo signal to drop to (1/e) of its initial value. This is also called T_2, although it does not have any place in the Bloch equations, which give exponential transverse relaxation. Examples of these two types of behavior are given in Ref. 37.

The relaxation in zero external field of Cu^{63} in Ni shows a behavior quite similar to the stimulated echo shown in Fig. 7. As in that case, the fast initial relaxation is attributed to nuclei near the center of the wall with large enhancement. The "bulk" relaxation rate of spins

far out in the wall is taken from the straight, large τ, data, which corresponds to exponential relaxation. This "bulk" T_2 of Cu^{63} in zero field was measured in the 2% and 2.5% samples at 4.2°K, 77°K, and 300°K. The values, in ms, are 4.2 ± .5, 0.50 ± .08, and 0.27 ± .07.

The behavior in the high field, high power regime is quite different. The relaxation rate is slower at short times than at long ones. This is seen in Fig. 13, which shows transverse relaxation measurements for Cu^{63} at 4.2°K in 6 kG field for the same four alloys in which longitudinal relaxation in the high field region was measured. This behavior contrasts with the longitudinal relaxation, which is exponential, except for effects of incomplete saturation, as shown in Fig. 10. If the transverse relaxation were exponential or Gaussian, the curves in Fig. 13 would be straight lines or parabolas, respectively. It is clear that they are not straight, nor parabolas, because they are not flat at $\tau = 0$. The curves were fitted with an arbitrary exponent, n, which corresponds to a relation:

$$A(t) = A_0 e^{-[(2\tau/T_2)^n]} \qquad \text{III-2}$$

Again, the data in Fig.13 cannot be well fitted by such a curve, because for $n > 1$, the curve is flat at $\tau = 0$ and the data are not. In order to fit the data, it was necessary to throw out the first point because of the non-flatness and the large weight of the small τ points in a log-log plot, after using it to determine the $\tau = 0$ intercept. This fit determines an exponent, n, and a time to decrease to (1/e) of the original signal, $T_{2,(1/e)}$. These parameters, chosen for the best fit, are shown for the data in the intermediate and high field region in Table 3.

It can be seen from Fig. 13 that the relaxation curves may approach a straight line at long times. For two reasons, it is difficult to tell whether this is actually the case. First, the signal-to-noise ratio is poorest for these weak signals. Second, it is always possible to fit a small portion of a curve by a straight line. With the exponents, as given in Table 3, in the range 1.0-1.5, it is hard to distinguish the curve from a straight line. The data at long times correspond well to the curve with the tabulated exponent. However, this is mainly due to the $\tau = 0$ intercept, which is included in the fit, while a straight line at long τ would correspond to a much higher intercept. A fit to a straight line was made for the data past a certain τ chosen by eye as corresponding to the straight portion. This fit determined the relaxation time, $T_{2,\infty}$, given in Table 3. The straight and curved fits shown in Fig. 15 seem to be about equally good for the long τ data.

B. Comparison with Theory

There can be contributions to the transverse relaxation from both spin-lattice and spin-spin interactions. Thus we can separate the transverse relaxation rate:

$$\frac{1}{T_2} = \left(\frac{1}{T_2}\right)_{\text{spin-spin}} + \left(\frac{1}{T_2}\right)_{\text{spin-lattice}} \qquad \text{III-3}$$

If T_2 obeys a relation $T_2T = \text{const.}$, this indicates that the transverse relaxation rate is dominated by spin lattice relaxation ($\propto T$) rather than spin-spin relaxation (weakly dependent on T). In ferromagnetic metals where this behavior is observed , it is often found that $(T_2T)^{-1}/(T_1T)^{-1} > 1$, e.g. for Ni^{61} in Ni, $T_1/T_2 \simeq 3$.[38] This is surprising in view of the fact that, as was seen in Chapter II, the spin-lattice relaxation in Ni is

dominated by the d-orbital mechanism. Since this mechanism is isotropic, one would expect $T_1 = T_2$. Walstedt[38] has explained the discrepancy by assuming that for, $I > 1/2$, the quadrupole broadening removes all but the $m = \pm 1/2$ transition from the observed resonance line. With this assumption, he obtains excellent agreement with the observed ratios. It is reasonable to assume at least as much quadrupole broadening in the Ni-Cu alloys, where the cubic symmetry is destroyed, as in pure Ni. Cu^{63} has the same nuclear spin as Ni^{61}, $I = 3/2$, so Walstedt's theory predicts the same ratio $T_1/T_2 = 3.2$, assuming that the signal comes entirely from the $\pm 1/2$ transition and that spin-spin interaction is negligible or subtracted out.

The transverse relaxation measured in zero field of Cu^{63} in the 2% and 2.5% Ni-Cu samples does not obey $T_2T = \text{const}$. From the values given in Section A for these samples, we find values of T_2T (in ms°K) equal to 18 ± 2, 38 ± 6, and 81 ± 18, for 4.2°K, 77°K , and 300°K, respectively. This is to be compared with $T_1T = 100$ ms°K. The shorter T_2T at 4.2°K may indicate the presence of spin-spin effects. Since $(\frac{1}{T_2})_{\text{spin-spin}}$ is relatively temperature independent, the effect of spin-spin contribution to T_2 is to lower T_2T at lower temperatures. However, from the spin-spin relaxation times we will deduce in connection with the high field transverse relaxation, it is clear that spin-spin interactions contribute negligibly to the T_2's measured at 77°K and 300°K. Yet even here, where spin-lattice relaxation dominates, we do not find $T_2T = \text{const}$. The 77°K value agrees roughly with Walstedt's predicted T_1/T_2. However, at 300°K, the situation appears nearer to $T_1 = T_2$. Similar behavior was reported[39] for Ni^{61} in Ni, for which at 1.5°K and 4.2°K, $T_1/T_2 \simeq 3$, while at 77°K and 295°K, $T_2 = T_1$

These measurements were also made in zero applied field, so that relaxation due to wall mechanisms is important. However, in high field, in the absence of domain wall complications, the observed T_1/T_2 is in good agreement with theory,[38] so that we may apply Walstedt's theory with some confidence in the high field, domain region.

Using Walstedt's estimate of the maximum contribution to transverse relaxation from spin-lattice relaxation and the observed T_1 of Chapter II, we can determine the relative importance of the spin-spin and spin-lattice mechanisms in the transverse relaxation measured in the high field region. From T_1T = 1.0 sec°K and T_1/T_2 spin-lattice = 3, we arrive at (T_2) spin-lattice = 80 ms and 160 ms for T = 4.2°K and 2.1°K respectively. These values are much longer than the observed T_2's at these temperatures shown in Table 3. This indicates that the transverse relaxation is dominated by spin-spin interactions.

Since the relaxation observed for Cu^{63} in Ni in the high field region is slower at first, it is not explicable in terms of successive signals from nuclei in different environments, as was the case in zero field. If this were the case, the slower relaxing (longer lived) signal would predominate at long times. Since the longitudinal relaxation of the high field signal was explicable in terms of a single type of environment, namely the saturated bulk, it is reasonable to expect the same to be true of the transverse relaxation of this signal. Assuming, therefore, that the transverse relaxation is homogeneous, it represents the Fourier transform of the homogeneous lineshape of the nuclei involved. The curves shown in Fig. 13, which are curved for small τ and then go over to straight exponential, suggest a lineshape which is Lorentzian with a cutoff. Physically, the cutoff corresponds to the

maximum interaction between spins. If we picture the transverse dephasing process as spins precessing in fields due to interactions with other spins, the maximum interaction implies a maximum rate at which spins can dephase. The exponential behavior at short times corresponds to few, fast relaxing spins way out in the wings of the Lorentzian line. With the cutoff, there are no such fast relaxing spins and the rate is slowed down at short times, as is observed.

The dominant spin-spin interaction in a ferromagnet is the Suhl-Nakamura interaction.[40] The Suhl-Nakamura mechanism couples nuclear spins by exchange of a virtual spin wave, to which they are coupled by the transverse hyperfine interaction, H = A I.S. The nuclear Hamiltonian for a cubic crystal is:[41]

$$S\text{-}N = \sum_{i \neq j} V_{ij} I_i^+ I_j^-, \qquad \text{III-4}$$

where the asymptotic form of V_{ij} is:

$$V_{ij} = -\left(\frac{A^2 S}{8\pi h \omega_e}\right)\left(\frac{a_o}{r_{ij}}\right) e^{-Kr_{ij}} \qquad \text{III-5}$$

in which $1/K = a_o \left(\frac{\omega_e}{\omega_a}\right)^{1/2}$

ω_e is the exchange frequency, given by: $\hbar\omega_e = 2JS$; ω_a is the sum of the electronic Zeeman and anisotropy frequencies, for a ferromagnet, and a_0 is the lattice spacing.

To estimate the cutoff in the homogeneous lineshape, we evaluate V_{ij} for next nearest neighbors. It is assumed that Cu atoms with a Cu nearest neighbor experience a quite different hyperfine field from that in an isolated Cu. Thus Cu-Cu pairs are shifted out of the observed resonance. Thus it is appropriate to use the next nearest neighbor distance to estimate the maximum interaction felt by observed nuclei. Pincus et al.[41] state that for $(\omega_e/\omega_a)^{1/2} >> 1$, which is satisfied in the present case, III-5 is valid for small Kr. It is questionable, however, that it is very good as close as next nearest neighbors. Nevertheless, III-5 gives a good enough estimate for this rough comparison.

For the quantities in III-5 which refer to spin waves, we use values for pure Ni, since the spin waves are not drastically affected by a few percent Cu. Thus, ω_e is evaluated using $\hbar\omega_e = 2JS$. J is determined from the coefficient of the Bloch $T^{3/2}$ law, $J = 230k_B$, S = 1/2,[42] giving $\omega_e = 3.0 \times 10^{13}$ sec^{-1}. A can be eliminated in favor of the known nuclear frequency due to the hyperfine interaction, $AIS = \hbar\omega_n I$, Thus taking $r_{ij} = \sqrt{2}\, a_o$, we get

$$V_{max}^{S-N} = \frac{\hbar\omega_n^2}{8\pi S\omega_e} \frac{1}{\sqrt{2}} \qquad \text{III-6}$$

$$\omega_{max}^{S-N} = \frac{\omega_n^2}{4\pi\omega_e} = 1.9 \times 10^2 \text{ sec}^{-1} \qquad \text{III-7}$$

By the Fourier transform argument, we expect the relaxation

curve to straighten for $2\tau \sim (\omega_{max})^{-1} = 5.2$ ms. This is in order of magnitude agreement with the estimated position of the beginning of the straight line fit in Fig. 13., which is about at $2\tau = 20$ ms. Considering the roughness of the above calculation, this is reasonable agreement.

Pincus et al.[41] have considered transverse relaxation due to the Suhl-Nakamura interaction, in the presence of inhomogeneous broadening. As an indicator of the lineshape, they use the ratio M_4/M_2^2, where M_n is the nth moment of the line profiles. This ratio equals 3 for a Gaussian line and is large for a cutoff Lorentzian line, approaching infinity for a pure Lorentz. For a homogeneous line and 100% concentration of like nuclear spins, they find a nearly Gaussian line. The inhomogeneous broadening detunes nuclei of different frequencies, inhibiting the Suhl-Nakamura interaction between them, since it is an energy conserving process. Thus, inhomogeneous broadening decreases all the moments. It decreases M_2^2 more than M_4 however. This is because the interaction is more effectively detuned by inhomogeneous broadening for distant spins, which feel a weaker interaction, as given by III-5. The strength of the S-N interaction at the nucleus involved is roughly the maximum allowable nuclear Zeeman energy non-conservation. The fourth moment is more sensitive to the strong, short range interaction and is thus less reduced by the long range detuning. Thus the ratio M_4/M_2^2 is increased, which leads to a nearly Lorentzian line. This effect is similar to a dilution of interacting spins, which was examined for dipole-dipole interactions by Kittel and Abrahams.[43] They find the transition from Gaussian to cutoff Lorentzian between 10% and 1%. In the present experiment, both inhomogeneous broadening and dilute Cu^{63} effects are present.

The Suhl-Nakamura second moment can be calculated, neglecting detuning from inhomogeneous broadening, using Van Vleck's formulation.[44] The second moment is linear in concentration, as the sum over sites occupied by the nuclei of interest can be replaced by c X the sum over all sites. Therefore:[41]

$$M_2 = \frac{I(I+1)c}{24\pi} \left(\frac{A^2 S}{\hbar^2 \omega_e}\right)^2 \left(\frac{\omega_e}{\omega_a}\right)^{1/2} \qquad \text{III-8}$$

Since we are going to compare this with the high field data we take $\omega_a = \gamma_e(H_o + H_a)$ with H_o = 6kG, H_a = 2kG. The rest of the quantities are obtained as in III-6 and we obtain:

$$\Delta\omega_{S-N} = \sqrt{M_2} = \sqrt{c} \times 6 \times 10^3 \text{ sec}^{-1} \qquad \text{III-9}$$

The experimental transverse relaxation rates, $1/T_{2,(1/e)}$ and $1/T_{2,\infty}$ are plotted in Figs. 14 and 15, respectively, as a function of c and $\sqrt{c}$. As can be seen in Table 3, the measured values of T_2 are not constant in the high field region, as was T_1, but show roughly a 5% increase between 6 kG and 8 kG. This increase can be explained by the ω_a term in III-8. Assuming, roughly, that $1/T_2 \propto \Delta\omega_{S-N}$, we expect $T_2 \propto \omega_a^{1/4}$. Using $\omega_a = \gamma_e(H_o + H_a)$, this predicts a 6% increase in T_2 between 6 and 8 kG, in good agreement with the observed value. The value used in Figs. 14 and 15 are an average high field value, appropriate to 6 kG, since data are available at this field for all the runs. Because spin-spin relaxation must disappear for extremely dilute samples, the rate for c = 0 is expected to be that due to spin-lattice relaxation, $(1/T_2)$ spin-lattice = $3.2/T_1$. This value is shown at c = 0 in Figs. 14 and 15. The most convincing concentration dependence is shown in Fig. 15 a),

$1/T_{2,\infty}$ vs $\sqrt{c}$. From the slope of Fig. 15 a), we find the experimental relation:

$$\frac{1}{T_{2,\infty}} = \sqrt{c} \times 0.75 \times 10^3 \text{ sec}^{-1} \qquad \text{III-10}$$

The concentration used in III-10 is the Cu concentration. However, what is of interest is the Cu^{63} concentration, since the Cu^{63} and Cu^{65} resonances do not overlap. Cu^{63} is 70% abundant, so we must convert III-10 into a fit to the square root of the concentration of Cu^{63} by the relation $\sqrt{c}_{tot} = \sqrt{c_{63}}/\sqrt{0.7}$. Thus we obtain the correct experimental fit:

$$\frac{1}{T_{2,\infty}} = \sqrt{c} \times 0.90 \times 10^3 \text{ sec}^{-1} \qquad \text{III-10'}$$

For a Gaussian lineshape, one has the relation:

$$\frac{1}{T_{2,(1/e)}} = \frac{1}{\sqrt{2}} \sqrt{M_2} \qquad \text{III-11}$$

Thus comparing III-10 and III-9 via III-11, we see that the rate predicted by the Suhl-Nakamura interaction, without considering inhomogeneous broadening, is about five times faster than the experimental value.

This comparison was chosen because Fig. 15a) shows the only reasonable concentration dependence. However, if we use the long time, exponential relaxation rate, we are assuming a cutoff Lorentzian lineshape. In this limit, $1/T_2$ is expected to be proportional to c, not $\sqrt{c}$.[41,43] Thus it is difficult to explain the fit. Nevertheless, the factor of five is a rough estimate of the weakening of the S-N interaction due to inhomogeneous broadening. An estimate of the amount of inhomogeneous broadening is given by considering the ratio $\frac{\Delta\omega_{inhomo}}{\Delta\omega_{S-N}}$. Using the value measured for Cu^{63} in Ni at low temperatures, Δf_{inhomo} = 350 kHz, and III-9 we find this ratio to be about 350. Only the microscopic part of

this inhomogeneous linewidth is effective in detuning the nuclei. Portis[45] shows that: $1/T_2$ is reduced from the S-N value by $\Delta\omega_{S-N}/\Delta\Omega$ where $\Delta\Omega$ is the microscopic part of the inhomogeneous linewidth. Since it is not known what part of the observed linewidth is microscopic, it can only be observed that the above factor of 350 is ample to explain the five-fold weakening of the S-N interaction.

A quantitative measure of the observed shape of the relaxation is the exponents listed in Table 3 which give the best fit to the curves in Fig. 13. As previously mentioned, these vary from about 1 to 1.5, where 1 corresponds to exponential relaxation and 2 to Gaussian. It is expected that in the present case, where the Cu^{63} is both dilute and quite inhomogeneously broadened, the exponent would be close to 1. However, the Kittel and Abrahams[43] calculation of the effect of dilution is for the case of the dipole-dipole interaction, which falls off as $1/r_{ij}^3$. Likewise, Narath[46] reports a transition of the transverse relaxation from Gaussian to Lorentzian for decreasing concentration of Ag in Pd. He indicates that the transition occurs somewhat above 10% Ag, in rough agreement with Kittel and Abrahams. In this case, the transverse relaxation times are much shorter than the longitudinal ones, and are presumably caused by the Ruderman-Kittel interaction.[47] (In Ni-Cu, this interaction is much weaker than the Suhl-Nakamura interaction.) This interaction of the nuclei through the conduction electrons also goes asymptotically as $1/r_{ij}^3$.

Since the transition from Gaussian to Lorentzian with decreasing concentration takes place as the nuclei go from significantly interacting with many other nuclei to only a few, it is to be expected that the

transition will occur sooner for shorter range interactions. A $1/r^3$ interaction is limited to very few neighbor shells. The Suhl-Nakamura interaction goes as $\frac{1}{r} e^{-Kr}$. Considering the increase in numbers of neighbors in a given shell, which is proportional to r^2, this interaction does not cut off until 1/K. Evaluating $1/K = a_0 \frac{\omega_e}{\omega_a}$ in the present experiment, we find a range of about 11 lattice constants, which is a much longer range. Thus it is expected that the relaxation will not have become exponential until lower concentrations than the 10% of references 43 and 46. However, there is also the large detuning effect from inhomogeneous broadening, which Pincus et al.[41] find is enough to make the relaxation exponential even with 100% nuclear concentration, as in the antiferromagnet MnF_2.

The experimental situation can be investigated by looking at the dependence of the exponent listed in Table 3 as a function of field, temperature, and concentration. The exponent increases slightly in the high field region, corresponding to the increase in T_2 previously mentioned. It is interesting that in the intermediate region, particularly at high frequencies, where wall effects are still important, the exponents are close to one. This agrees with the exponential relation observed at long time for spins in the wings of the walls. The exponent is independent of temperature within experimental error, at 2.1°K and 4.2°K. At 77°K, the exponent decreases, but here, it is expected that spin-lattice relaxation becomes appreciable, so the situation becomes complicated. The exponents for 6 kG at helium temperatures are roughly 1.30, 1.45, 1.4, 1.48 for 1%, 2%, 2.5% and 5%. Thus, the concentration dependence is in the expected direction, closer to 1 for lower concentration.

In conclusion, we have attributed the low-temperature, high-field transverse relaxation to spin-spin interactions because of the large T_1/T_2 ratio and the slight temperature dependence of T_2 in the 2.1°K to 4.2°K region. The relaxation is observed to be intermediate between exponential (Lorentzian) and Gaussian behavior. The data can be interpreted as a curve with intermediate exponent or as a cutoff Lorentzian, which may be equivalent. The fact that non-Lorentzian behavior is observed at concentrations for which systems in which dipole-dipole interactions dominate are Lorentzian, is attributed to the longer range of the Suhl-Nakamura interaction. The observed relaxation rate is smaller than calculated from the Suhl-Nakamura second moment. This difference is attributed to detuning of nuclei by inhomogeneous broadening, which prevents them from interacting by the S-N interaction. It is not understood why this detuning does not produce a Lorentzian line, as predicted by Pincus et al.[41] Although the samples were homogenized, as described in Chapter II, it is possible that the Cu atoms are not randomly distributed. If they tend to cluster, the effective concentration is higher, and one would expect a more Gaussian line. Another possible source of disagreement is the calculation of the Suhl-Nakamura interaction in an alloy. Eq. III-5 was calculated for a homogeneous medium. In the case of a Cu nucleus in Ni-Cu, the coupling through the hyperfine field to the d band is not as direct as for Ni, assuming that the Cu has no moment. Thus although the S-N is expected to have the same asymptotic form as III-5, the coefficient would have to be determined to match the strength of the interaction at short range. Thus, it is possible that the detuning by inhomogeneous broadening is less

effective in changing the lineshape. Thus, the observed transverse relaxation of Cu^{63} in Ni-Cu has not been explained, although it is clear that spin-spin effects are involved.

Chapter IV

APPARATUS

A block diagram of the experimental setup is shown in Fig. 16. The oscillator is an Arenberg PG 650 pulsed oscillator, which nominally delivers 100 watts of r.f. power. The narrow band preamplifier and wide band amplifier are also made by Arenberg.

The sample matching network is shown in Fig. 17. The diodes are 1N3728, which have a typical high impedance $(\frac{dV}{dI})$ at low voltages and small impedance at high voltages. The purpose of these diodes and the $\frac{\lambda}{2}$ and $\frac{\lambda}{4}$ cables is to direct the r.f. input into the sample, thereby also reducing the amplifier saturation, and to direct the r.f. signal to the pre-amp. The diodes at the oscillator act like a short for the high level r.f. input pulses, so have no effect at this time. Likewise the diodes at the pre-amp look like a short. However, by transmission line theory, a short circuit is transformed into an open circuit a quarter wavelength away. Therefore at the junction to the sample, the connection to the pre-amp looks like an open circuit, so most of the r.f. goes down to the sample. For the very low voltage echo signal, the diodes act like a high impedance. The diodes at the pre-amp, which are in parallel to ground, have little effect. The diodes at the oscillator are in series and transformation by the $\frac{\lambda}{2}$ line leaves them unchanged, looking like a high impedance. Therefore most of the echo signal goes to the pre-amp. The actual effect of this network is not as dramatic as the above explanation promises, but it is a worthwhile improvement.

In order to achieve optimal matching to the sample, it is necessary that the line leading to it be terminated in its characteristic impedance, in this case 50 Ω. The sample is in the coil of a resonant

circuit to enhance the input and output voltages by the Q of the circuit. A capacitor, tunable from the outside, completes the resonant circuit. At resonance, the reactive components of the coil and capacitor cancel, leaving a purely resistive impedence due to the losses in the sample. For a single layered coil, whose length is about 1 1/2 times the diameter, the Q at 52 MHz was found to be about 12. This was, of course, with a Ni-Cu sample filling the coil. The number of turns was adjusted to give a value of L so that:

$$R = \omega L/Q \simeq 50\ \Omega \qquad \text{IV-1}$$

This condition was satisfied for a 10 turn coil having an inductance of 1.8 μH. With the sample resonant circuit matched to the characteristic impedence of the coaxial line leading down into the dewar, the length of this line is immaterial.

The variable attenuator after the amplifier is used to measure the signal amplitude accurately, which is crucial in measuring the relaxation rate. Since the Arenberg is a pulsed, not gated, oscillator, it was impossible to use phase coherent detection, which assures linearity. The diode detector and video amplifier in the Arenberg receiver was found to be nearly square law over a wide range. However, rather than depend on this power law, the 40 dB amplifier and precision variable attenuator were introduced between the amplifier and detector. The Arenberg amplifier was found to be linear over a wide range for sufficiently low gain. As the signal strength decreased, the attenuation was decreased to keep the r.f. level at the detector approximately constant. Since the attenuator varied in steps of 1 dB, there had to

be small variations in the detected signal strength. For this small range, the power law of the detector was determined with confidence, and a small correction made to the signal strength read from the attenuator.

A boxcar integrator, produced by the Physics Department Electronics Shop, was used to improve the signal-to-noise ratio. The echo width was of the order of a microsecond. The boxcar gate width was also of the same order. Stability of better than 0.1 μs was thus necessary to keep the boxcar gate positioned on the echo. The relaxation times, and hence pulse separations, were on the order of tens of milliseconds. Thus the pulse separation had to be stable to 1 part in 10^5. This is beyond the capability of analogue pulse delay units, such as the Tektronix 160 series. Therefore the Physics Department Electronics Shop designed and built for me a digital pulse delay unit based on the stability of a 1 Mc crystal oscillator. This unit puts out pulses with a set separation to trigger the oscillator and a pulse to trigger the boxcar an equal time later, for a T_2 measurement, or a pulse to start the echo train a set time after the last saturating pulse in the T_1 configuration. This digital delay unit gave crystal oscillator accuracy and stability (better than 5 parts in 10^6/day) to the crucial, long time intervals, while all the other less crucial, time intervals, such as the r.f. pulse widths, were generated by analogue devices.

In the high field region, maximum r.f. power was desired to excite the whole line and achieve the desired turning angles for the spins in the domain bulk. With the matching network described above, instantaneous power dissipation of about 1 kW was achieved. In the T_1 experiment at 77°K, the saturation pulses took up 150 μs of a 50 ms

period, or a duty ratio of 3×10^{-3}. In this case, the average power dissipated was 3 watts. In the more frequently encountered situation at helium temperatures, where the relaxation times, and hence periods, were longer, the average power dissipation was about 0.1 watt. In order to assure temperature stability with this much heat generated, the powdered samples were embedded in Apiezon N-Grease, which is easily penetrated by the powder at 100°C. At the experimental temperatures, the N-Grease freezes and has a high thermal conductivity, thus facilitating the heat transfer to the liquid (He or N_2) in which the sample is immersed. The sample fitted snugly, but open, in the coil. To assure free flow of cooling liquid about the sample, the can in which the sample coil and tuning capacitor were located had double side walls of Cu screen about 1/8" apart. This allowed the liquid in, while effectively screening out r.f. noise, particularly television signals, whose band starts at 54 MHz.

ACKNOWLEDGMENTS

I would like to thank Professor Alan Portis for suggesting the topic of this research and giving me many ideas for executing the experiment. He was also very generous with his help in interpreting the results. I would like to acknowledge a conversation with Dr. R. E. Walstedt concerning his relaxation measurements in Ni. In addition, Drs. P. Pincus and A. Narath and I had very helpful discussions about my experimental results, and I got much valuable information from a pre-print kindly sent by Dr. Pincus. It is my pleasure to thank Boris Chornik for his help in developing the sample making apparatus and for his help in preparing the samples. Al George and Will Simard of the Physics Department Electronics Shop were indispensible in producing the digital delay system and boxcar integrator. I would like to take note of the help provided by Professor Hahn's students in mastering the techniques associated with spin echoes. I am indebted to the National Science Foundation and the Atomic Energy Commission for the financial support provided during my graduate studies. Finally, I thank my wife, Rochelle, for her moral and material help with my experiment and thesis.

REFERENCES

1. Charles Kittel, Introduction to Solid State Physics third edition (1966) p. 462.
2. Ibid., p. 580.
3. Ibid., p. 463.
4. The low temperature specific heat yields $N_d(E_F) + N_s(E_F)$. $N_s(E_F)$ can be calculated using the free electron approximation. Or else, the value of $N_s(E_F)$ of Cu from its low temperature specific heat can be adjusted to Ni by taking account of the difference in number of s-electrons (see Chapter III, and Ref. 10). With the latter method, we estimate for Ni, $N_d(E_F)/N_s(E_F) = 11$.
5. A. C. Gossard and A. M. Portis, Phys. Rev. Lett. 3, 164 (1959). A. M. Portis and A. C. Gossard J. Appl. Phys. 31, 205S (1960).
6. S. S. Hanna, J. Heberle, G. J. Perlow, R. S. Preston and D. H. Vincent, Phys. Rev. Lett. 4, 513 (1960).
7. A. J. Freeman and R. E. Watson in Magnetism IIA. (Ed. Rado and Suhl), (1965) pp. 271-2.
8. E. L. Hahn, Phys. Rev. 80, 580 (1950).
9. Freeman and Watson, ibid. pp. 270-80.
10. T. Moriya, J. Phys. Soc. Japan 19, 681 (1964). Correction must be made for a factor of two error in the densities of states as pointed out by R. E. Walstedt, V. Jaccarino, and N. Kaplan, J. Phys. Soc. Japan 21, 1843 (1966) and tabulated in Ref. 27.
11. M. Weger, Thesis, University of California (1960), unpublished.
12. C. Kittel and J. K. Galt, Solid State Physics 3, 479 (1956).
13. D. S. Cowan and L. W. Anderson, Phys. Rev. 135, A 1046 (1964).
14. M. B. Stearns preprint (1968), "Relaxation of Domain Wall Nuclear

Spins Via Magnon Interactions in Fe."

15. M. Weger, Phys. Rev. 128, 1505 (1962).

16. A. G. Redfield, Phys. Rev. 96, 1787 (1955).

17. R. Gabillart, Comptes Rendu 232, 324 (1951).

18. M. B. Stearns and A. W. Overhauser, J. Appl. Phys. 39, 440 (1968).

19. N. Kaplan, V. Jaccarino and J. H. Wernick, Phys. Rev. Lett. 16, 1142 (1966).

20. A. C. Gossard, A. M. Portis, M. Rubinstein and R. H. Lindquist, Phys. Rev. 138, A 1415 (1965).

21 R. M. Bozorth, Ferromagnetism (1961) p. 569.

22. R. M. Bozorth and D. M. Chapin, J. Appl. Phys. 13, 320 (1942).

23. A. Narath, Phys. Rev. 162, 320 (1967).

24. V. Jaccarino, N. Kaplan, R. E. Walstedt and J. H. Wernick, Phys. Lett. 23, 514 (1966).

25. R. E. Walstedt, private communcation. $T_1^{-1}{}_{,H=0}/T_1^{-1}{}_{,H} >> 4\pi M/3 = 0.69$ $(T_1{}_{,H=0}T)^{-1} \simeq 8\ \mathrm{sec}^{-1}{}^{\circ}\mathrm{K}^{-1}$.

26. M. H. Bancroft, Bull. Am. Phys. Soc. 13, 505 (1968).

27. M. B. Salamon, J. Phys. Soc. Japan 21, 2746 (1966).

28. Y. Obata, J. Phys. Soc. Japan 18, 1020 (1963).

29. M. Kontani and J. Itoh, J. Phys. Soc. Japan 22, 345 (1967).

30. N. Bloembergen, Physica 15, 588 (1949).

31. A. G. Redfield, Phys. Rev. 98, 1787 (1955).

32. A. G. Anderson and A. G. Redfield, Proceedings of the Fifth International Conference on Low Temperature Physics and Chemistry, Madison (1957).

33. T. Sugawara, J. Phys. Soc. Japan 14, 643 (1959).

34. A. Abragam, The Principles of Nuclear Magnetism (1961), p. 358.

35. J. Korringa, Physica 16, 601 (1950).

36. D. Pines, Solid State Physics 1, 366 (1955).

37. A. Narath, A. T. Fromhold, and E. D. Jones, Phys. Rev. 144, 428 (1966).

38. R. E. Walstedt, Phys. Rev. Lett. 19 146 (1967).

39. M. Weger, E. L. Hahn, and A. M. Portis, J. Appl. Phys. 32, 124S (1961).

40. H. Suhl, Phys. Rev. 109, 606 (1958). T. Nakamura, Prog. Theor. Phys. 20, 542 (1958).

41. P. Pincus, V. Jaccarino, D. Hone, and Tin Ngwe, Phys. Lett. 27 54 (1968). Tin Ngwe, D. Hone, V. Jaccarino and P. Pincus, forthcoming in the Phys. Rev.

42. Charles Kittel Introduction to Solid State Physics, 2nd ed., p. 407.

43. C. Kittel and E. Abrahams, Phys. Rev. 90, 238 (1953).

44. J. H. Van Vleck, Phys. Rev. 74, 1168 (1948).

45. A. M. Portis, Phys. Rev. 104 584 (1956).

46. A. Narath, J. Appl. Phys. 39, 553 (1968).

47. M. A. Ruderman and C. Kittel, Phys. Rev. 96, 99 (1954).

TABLE I

C. W. Saturation Determinations of T_1 of Cu^{63} in Cu

Reference	Year	Temperature Range (°K)	T_1T(sec°K)
30	1949	1.15-20.2	0.33
31	1955	room temperature	0.90 ± .18
32	1957	1.35-4.2	1.27 ± .10
33	1958	1.4-85	0.80 ± .15

Averaging last three values, we get $T_1T = 0.97 \pm .20$

or $(\gamma_n^2 T_1 T)^{-1} \times 10^7 = 0.20 \pm 0.04$

TABLE II

Theoretical Determination of T_1 from Knight Shift

Method	$(\gamma_n^2 T_1 T)^{-1} \times 10^7$	$T_1 T$
Korringa relation	0.29	0.69
Pines collective theory	0.17	1.20

TABLE III

Concentration (%)	Temperature (°K)	Field (kG)	n	$T_{2,(1/e)}$(ms)	$T_{2,\infty}$(ms)
		6	1.31 ± .06	20.6 ± .5	12.4 ±.1
1	2.1	8	1.48 ± .04	22.5 ± .5	12.4 ±.1
		4	1.25 ± .06	14.2 ± .2	9.5
1	4.2	6	1.30 ± .06	15.2 ± .3	9.7
		8	1.32 ± .10	15.8 ± .3	9.0
		2(h)	1.02 ± .04	3.04 ± .05	3.0 ±.1
		2(l)	1.20 ± .19	11.0 ± .5	6.7 ±
2	2.1	4	1.32 ± .12	12.0 ± .4	7.4 ±.3
		6	1.49 ± .08	15.7 ± .4	7.2 ±.1
		4	1.31 ± .02	12.7 ± .1	8.0 ±.15
2	4.2	5	1.40 ± .02	13.9 ± .2	7.2 ±.2
		6	1.44 ± .02	14.7 ± .1	8.0 ±.15
		3(h)	1.26 ± .09	11.7 ± .3	7.9 ±.5
		3(l)	1.19 ± .05	12.4 ± .2	8.8 ±.4
2.5	2.1	6	1.46 ± .06	17.0 ± .3	9.0 ±.1
		8	1.37 ± .12	17.6 ± .6	9.4 ±.1
		2(h)	1.15 ± .02	8.2 ±.1	6.5 ±.06
		2(l)	0.99 ± .05	8.0 ±.2	8.0 ±.15
		4(h)	1.35 ± .03	12.1 ± .1	7.6 ±.1
2.5	4.2	4(l)	1.30 ± .04	11.5 ± .1	7.8 ±.1
		6	1.35 ± .05	12.4 ± .1	6.5 ±.15
		7	1.34 ± .08	12.6 ± .15	7.7 ±.2
		8	1.32 ± .06	13.1 ± .2	9.1 ±.2
		6	1.48 ± .06	14.5 ± .3	6.3 ±.2
5	2.1	8	1.56 ±.04	16.1 ± .1	6.7 ±.1
		2(h)	0.97 ± .10	3.9 ±.2	4.7 ±.1
		4(h)	1.49 ± .03	10.7 ± .1	5.2 ±.1
5	4.2	4(l)	1.33 ± .07	9.2 ±.2	4.9 ±.1
		6	1.49 ± .04	10.8 ± .1	5.0 ±.1
		8	1.52 ± .05	11.4 ± .1	5.1 ±.1
		4	1.24 ± .08	1.97 ± .05	1.65 ±.1
5	77	6	1.33 ± .06	2.14 ± .05	1.35 ±.2
		8	1.39 ± .10	2.64 ± .08	1.80 ±.1

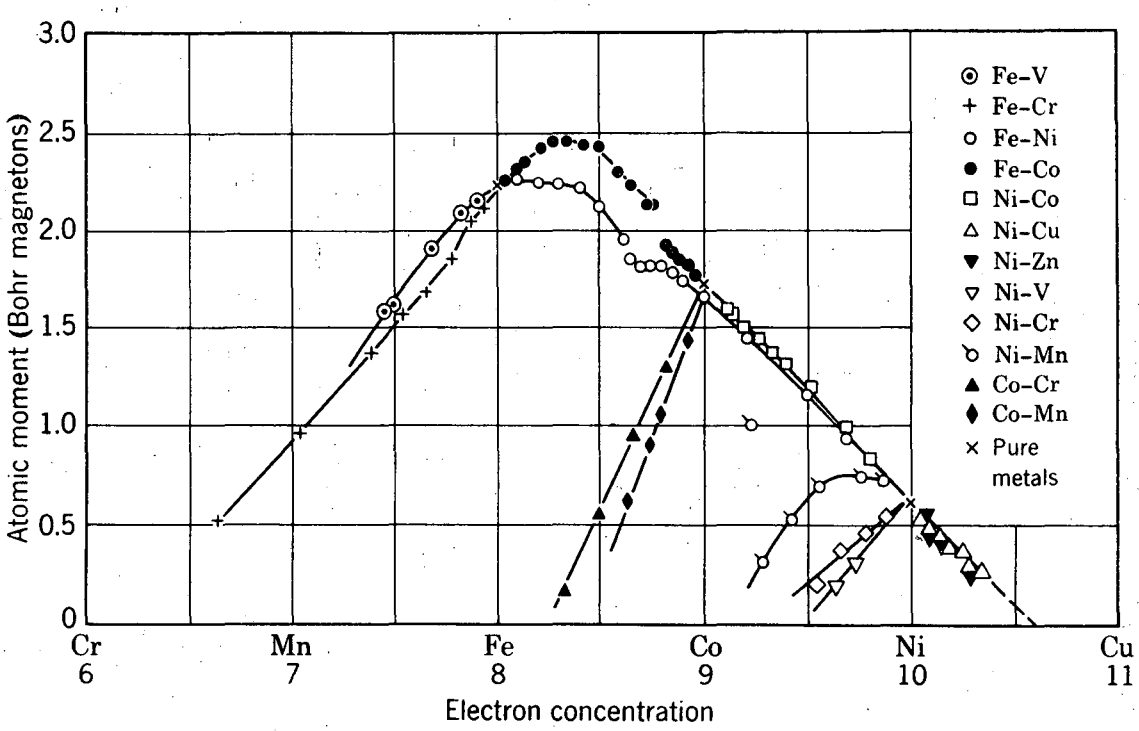

Fig. 1: Slater-Pauling diagram, showing the average atomic moments of binary alloys of the elements in the iron group. From Kittel, Introduction to Solid State Physics, 3rd edition.

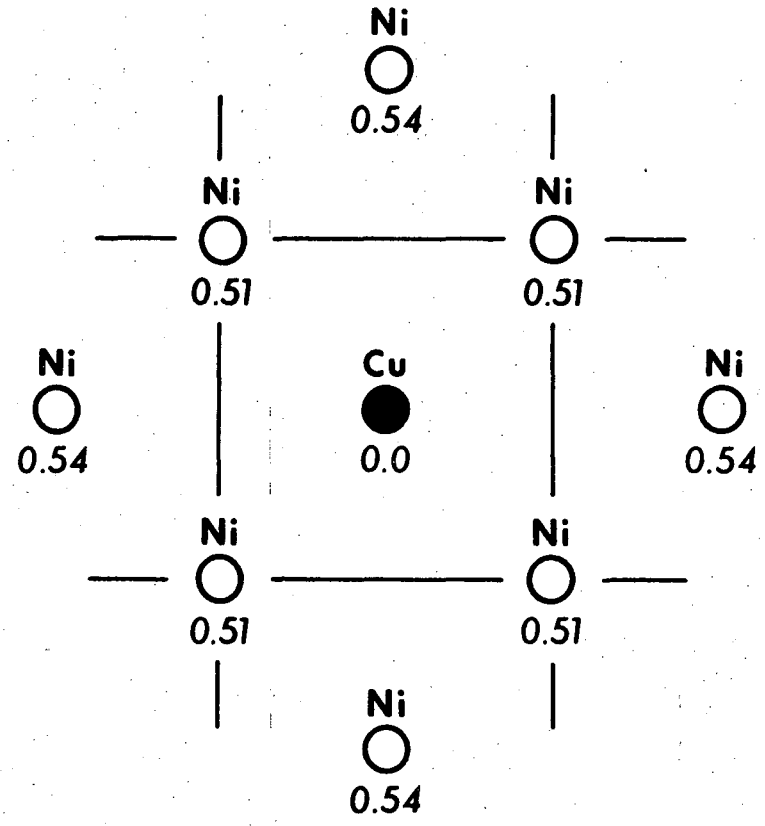

Fig. 2: Cross section of an isolated Cu atom in Ni. The numbers indicate the average number of holes in the d shell assumed in the screening model.

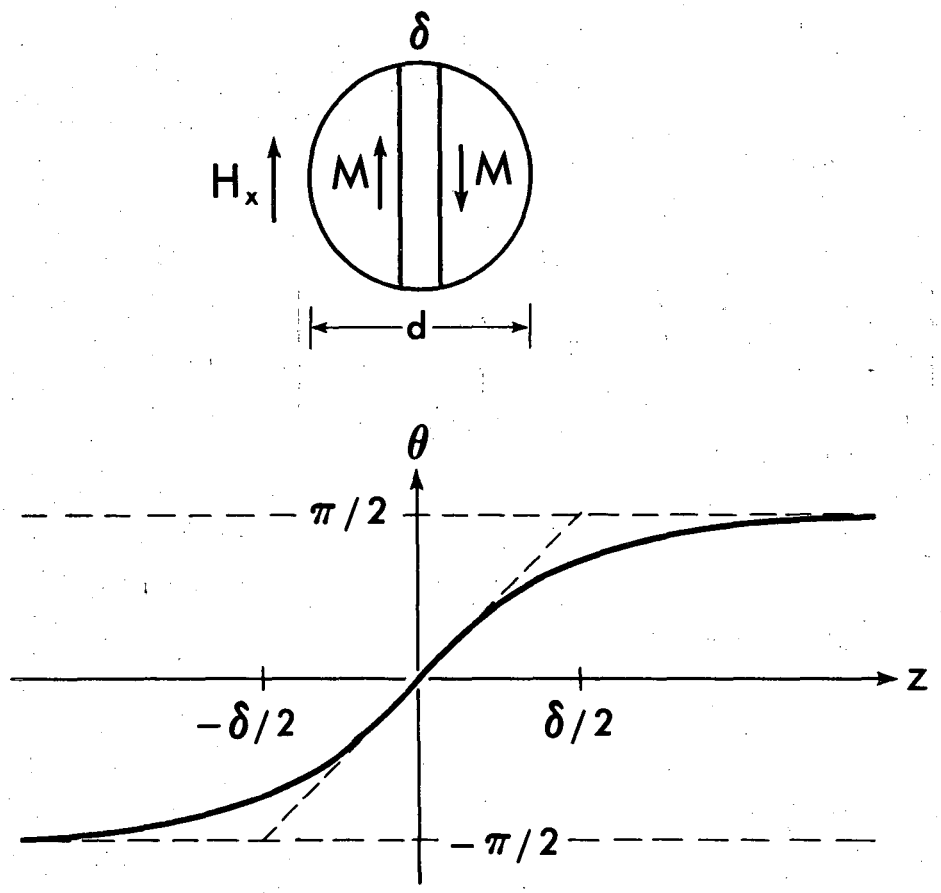

Fig. 3: a) Spherical ferromagnetic particle with a 180° Bloch wall.
b) Direction of the magnetization versus position for a 180° Bloch wall.

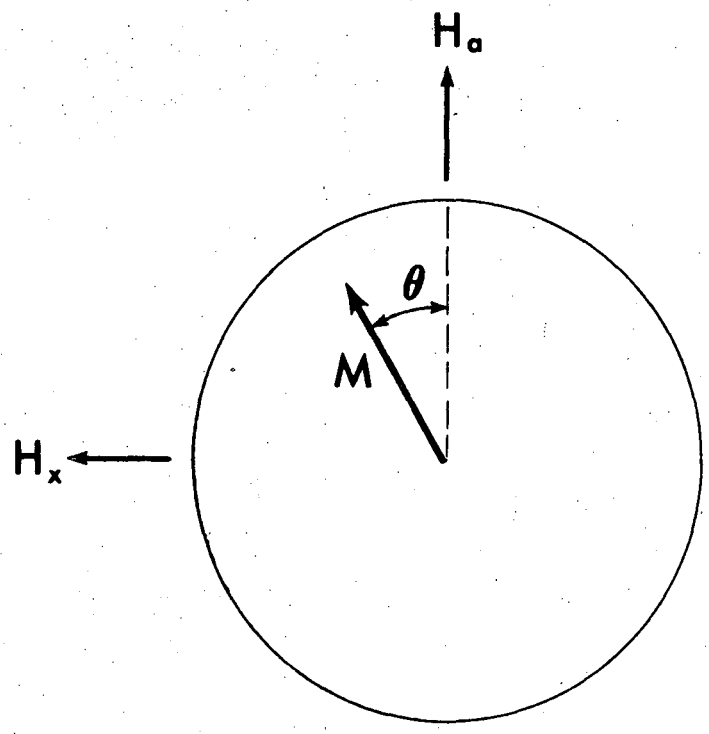

Fig. 4: Saturated or single domain spherical ferromagnetic particle.

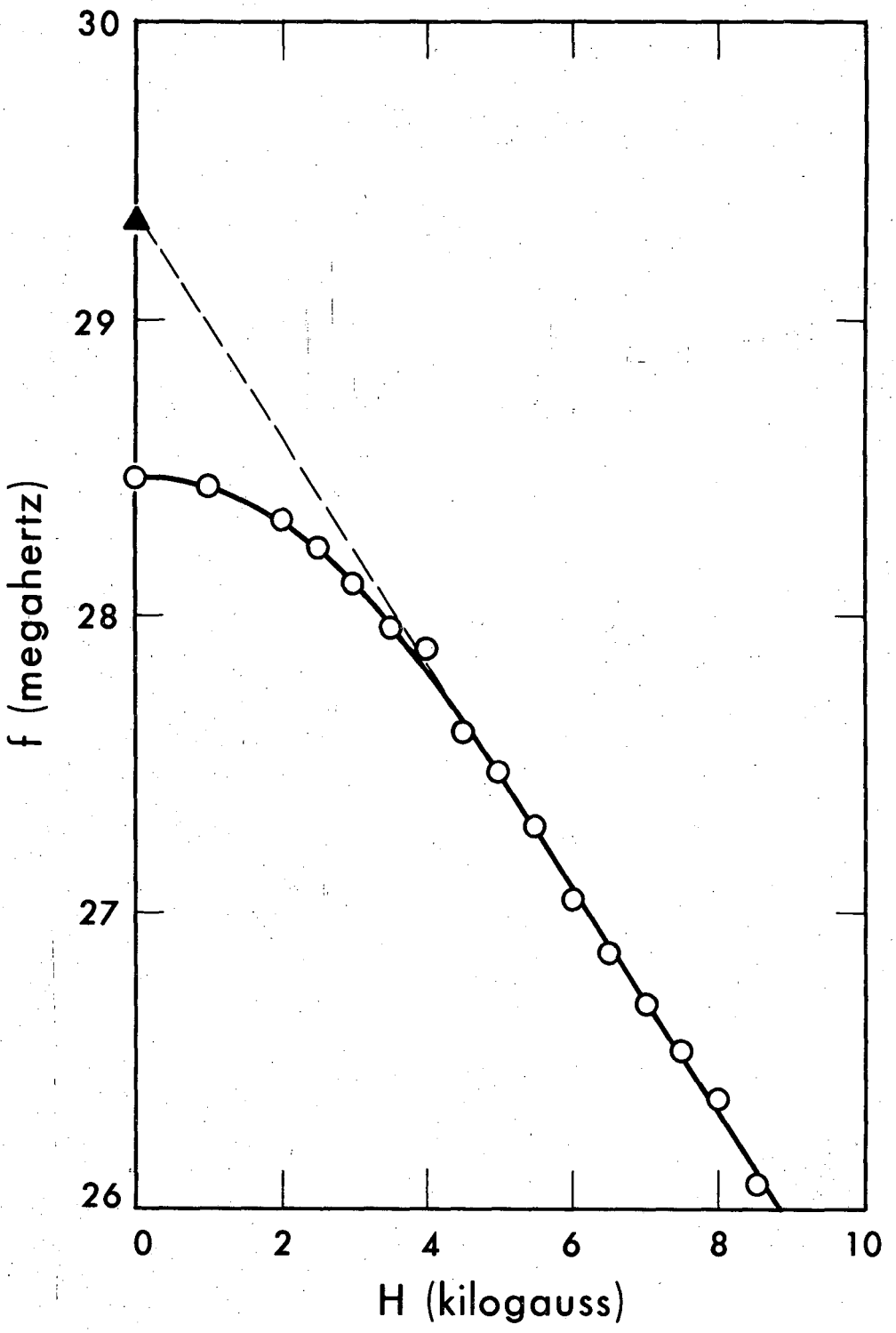

Fig. 5: Resonant frequency versus external field for Ni^{61} in Ni sponge. The ▲ indicates the calculated intercept of the high-field extrapolation.

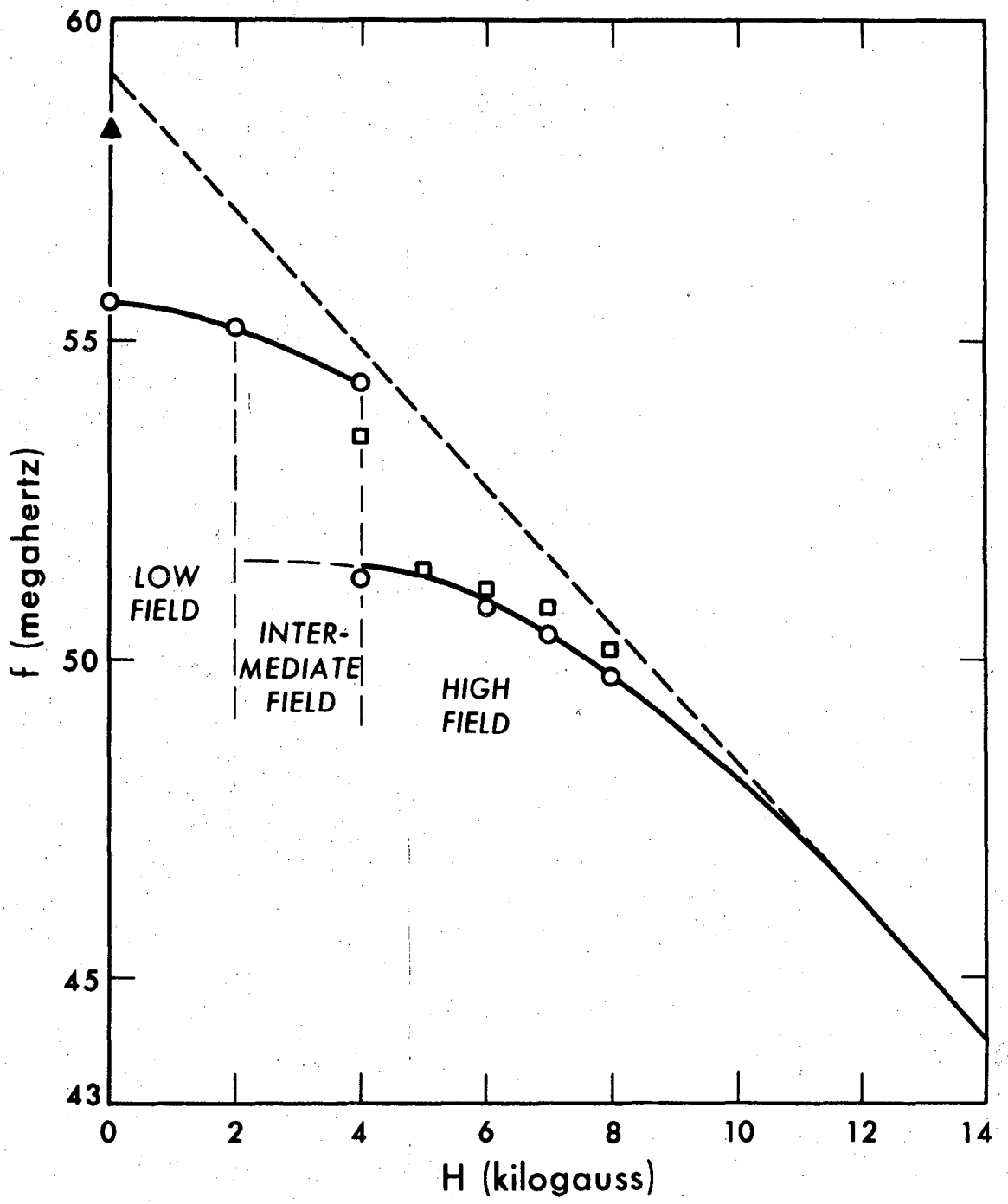

Fig. 6: Resonant frequency versus external field for Cu^{63} in 2% Ni-Cu. The ▲ indicates the calculated intercept of the high-field extrapolation.

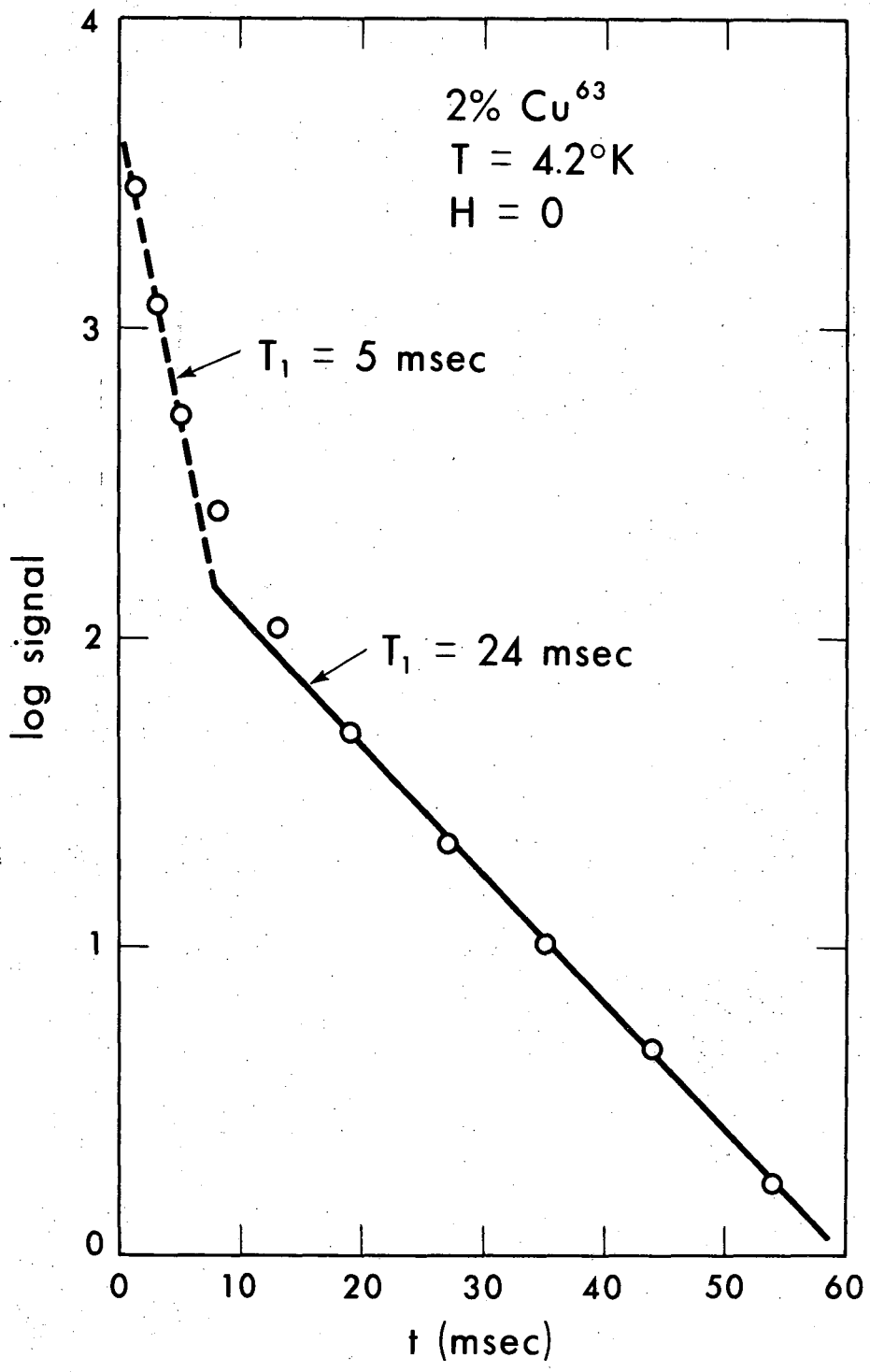

Fig. 7: Log of the zero-field stimulated echo signal of Cu^{63} versus time.

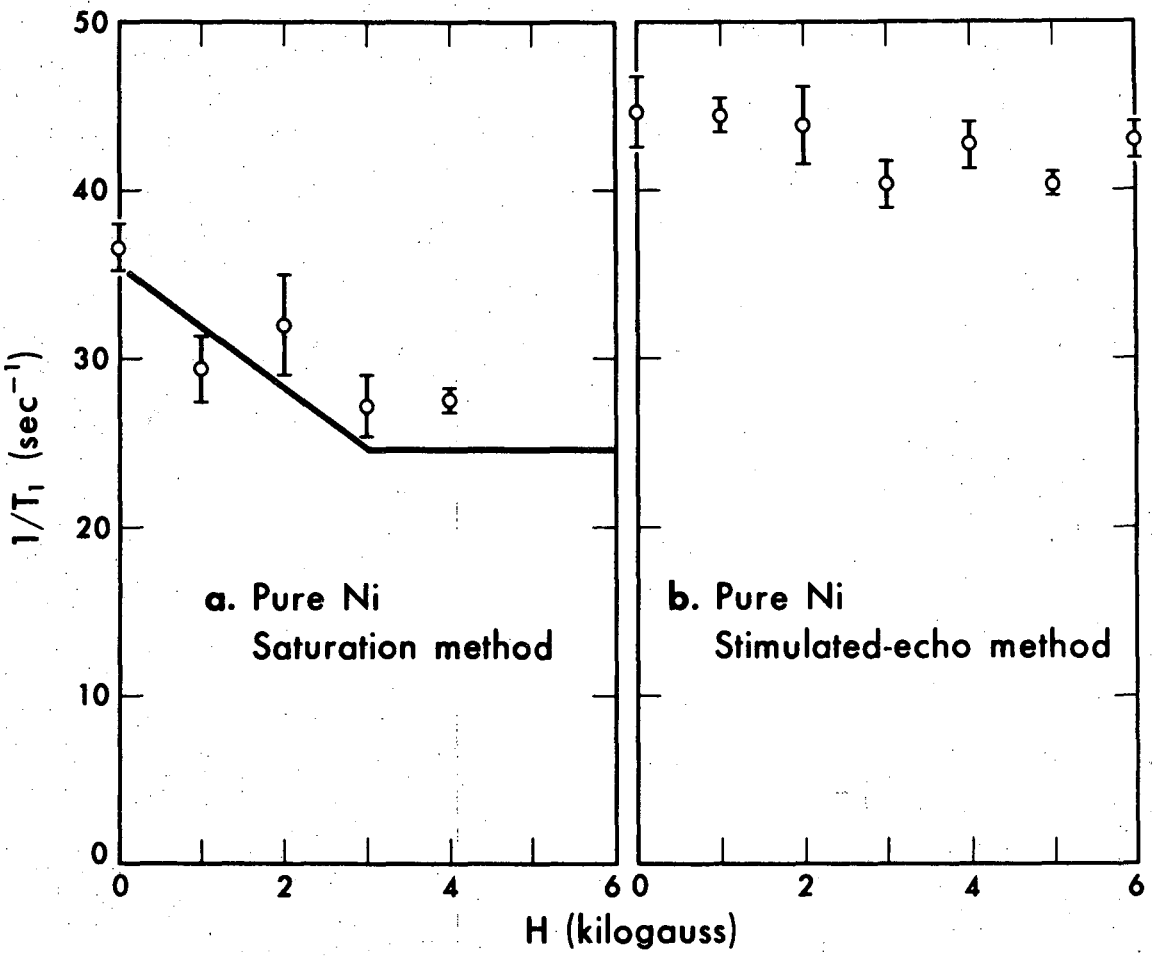

Fig. 8: Comparison of the field dependence of the longitudinal relaxation rate of Ni^{61} measured by: a) the saturation and b) the stimulated echo technique.

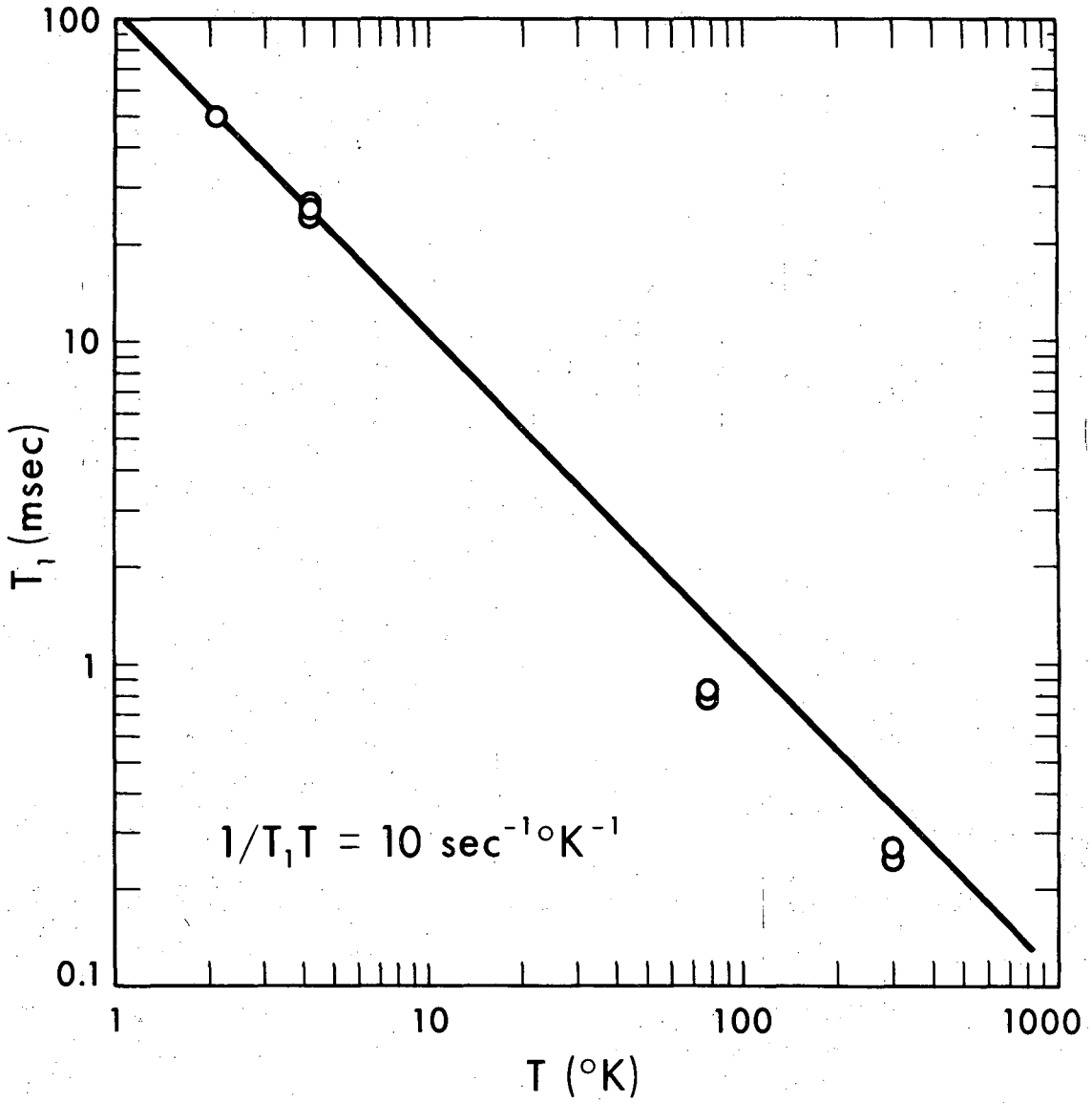

Fig. 9: Zero-external field longitudinal relaxation time of the Cu^{63} in 2% Ni-Cu versus temperature. The 45° line represents T_1T = const.

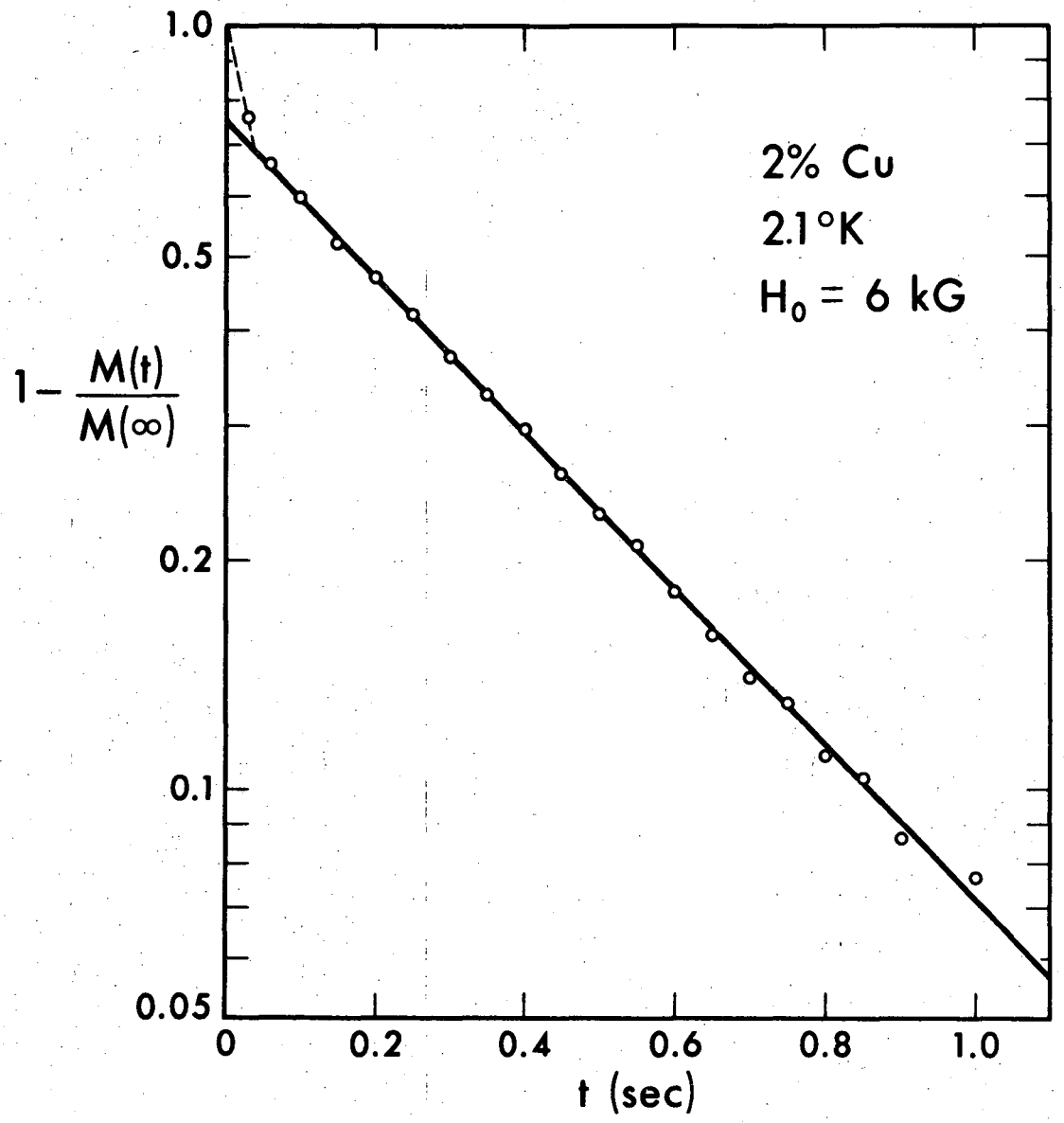

Fig. 10: High-field longitudinal relaxation of Cu^{63} measured by the saturation method.

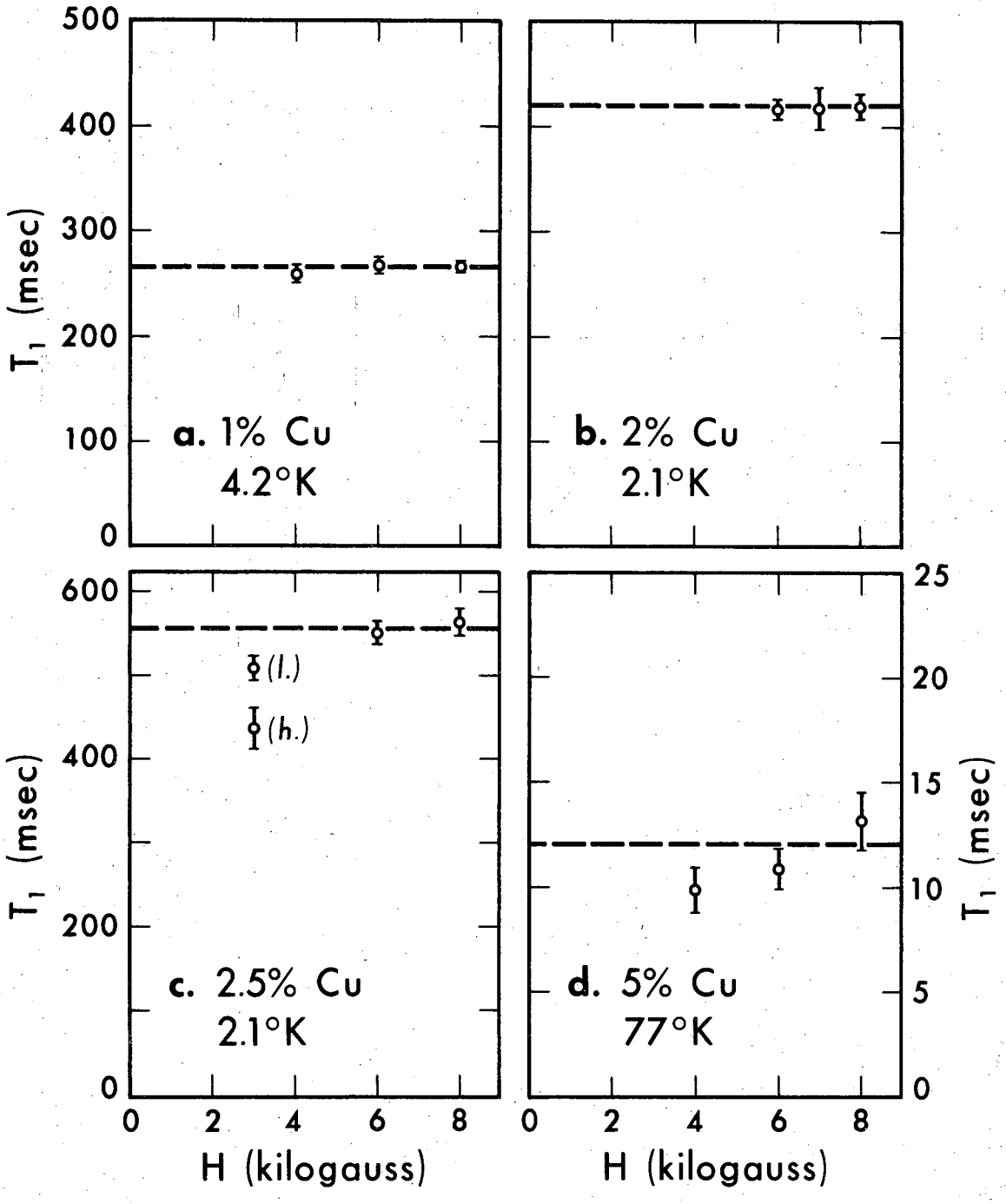

Fig. 11: Field dependence of the Cu^{63} intermediate- and high-field longitudinal relaxation times for various concentrations and temperatures.

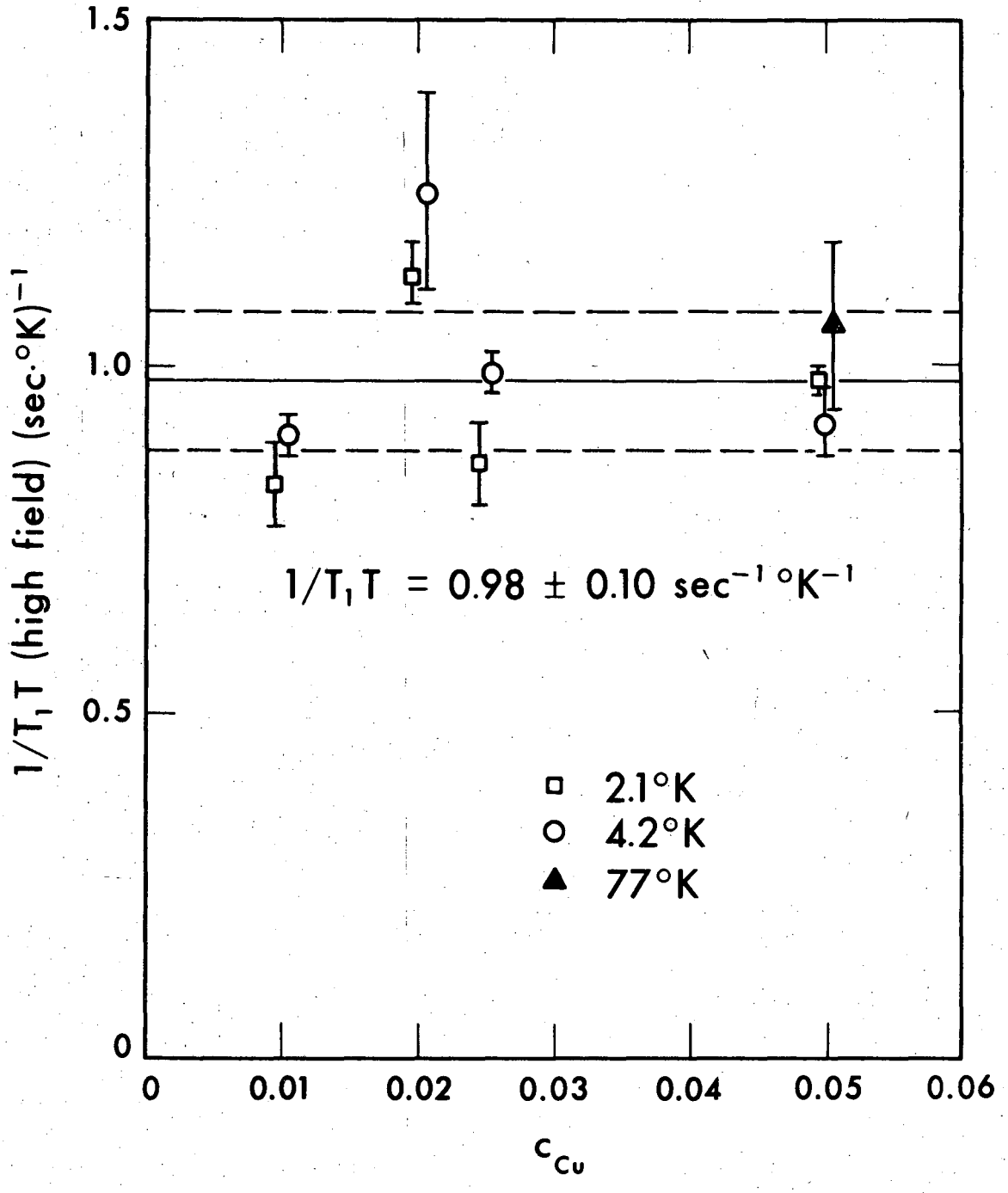

Fig. 12: Mean high-field $(T_1T)^{-1}$ of Cu^{63} in Ni-Cu versus Cu concentration and temperature.

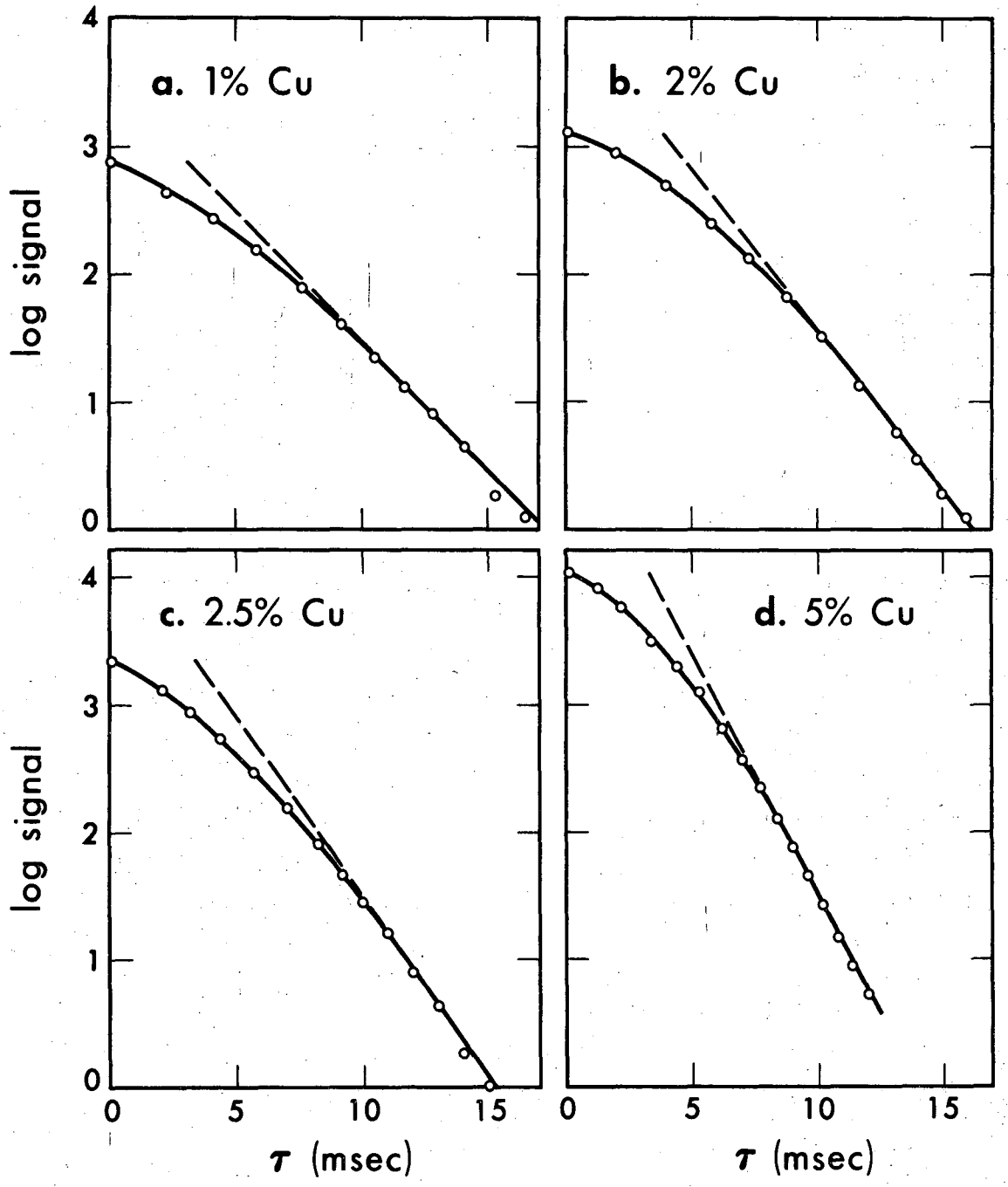

Fig. 13: Transverse relaxation of Cu^{63} in Ni-Cu at 4.2°K in a 6 kG external field in the four samples investigated.

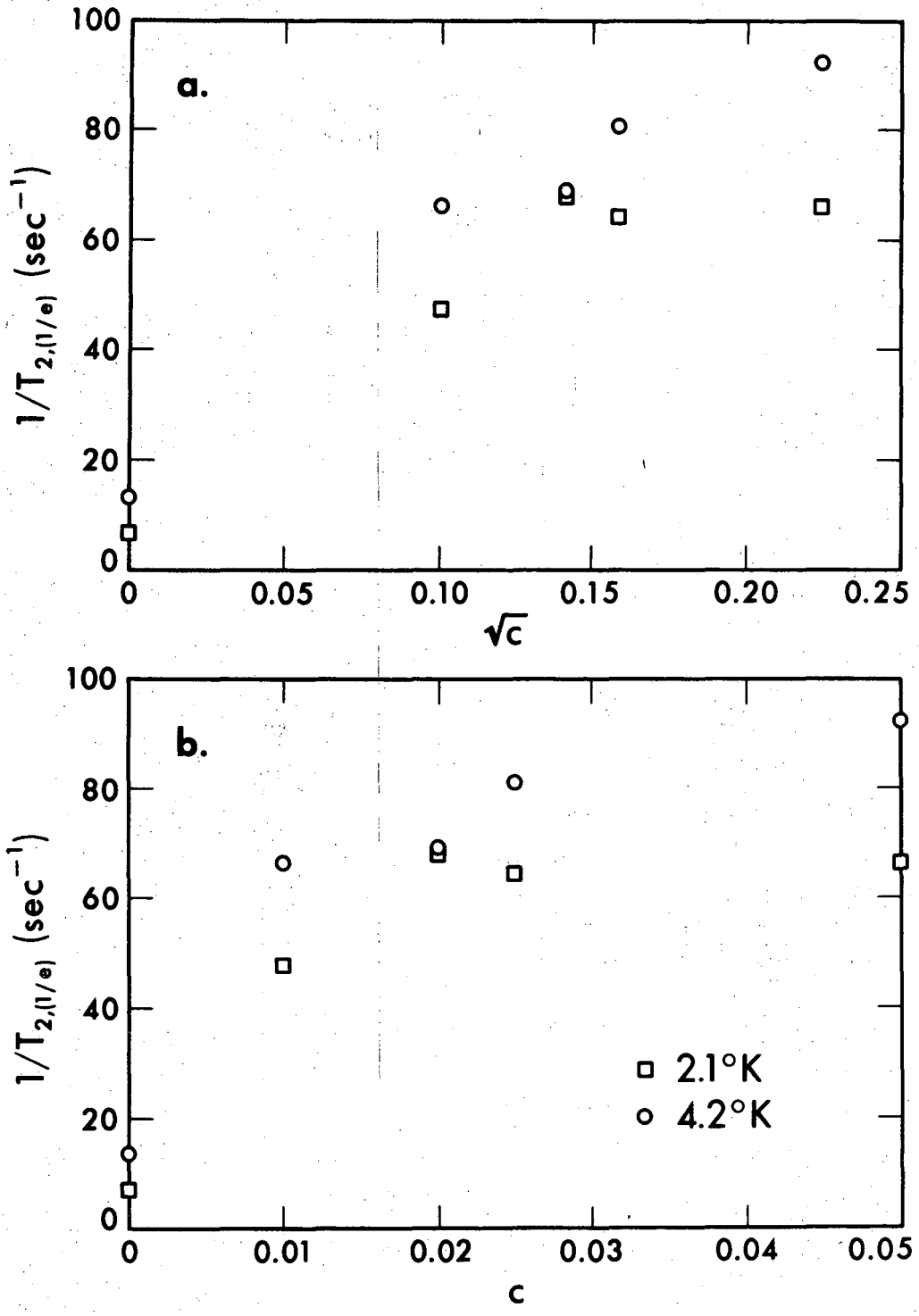

Fig. 14: Time for the Cu^{63} spin echo to fall to (1/e) of its amplitude versus temperature and a) the square root of the Cu concentration and b) the Cu concentration.

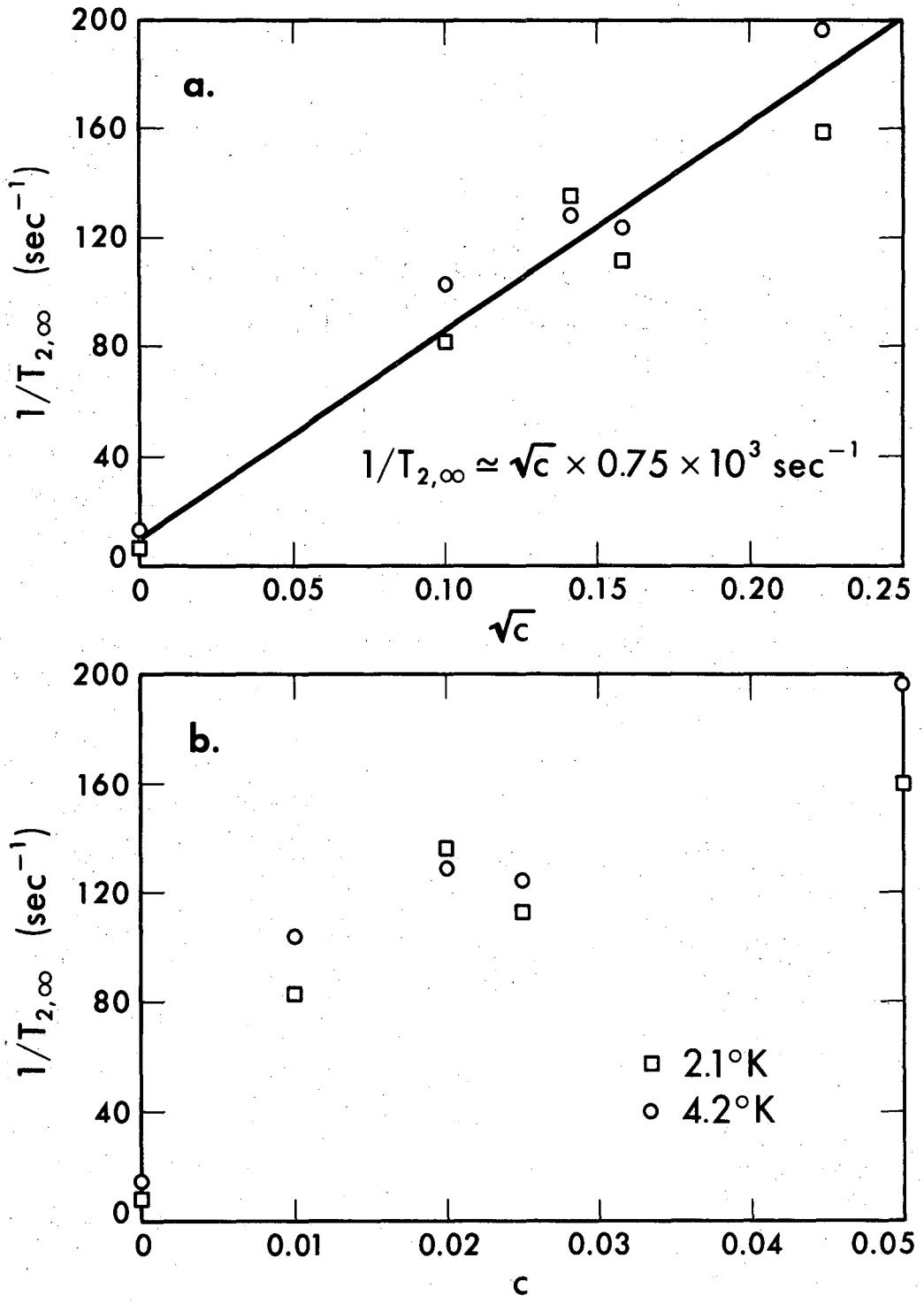

Fig. 15: Exponential relaxation time of Cu^{63} fitted to the long τ data of Fig. 13 versus temperature and a) the square root of the Cu concentration and b) the Cu concentration.

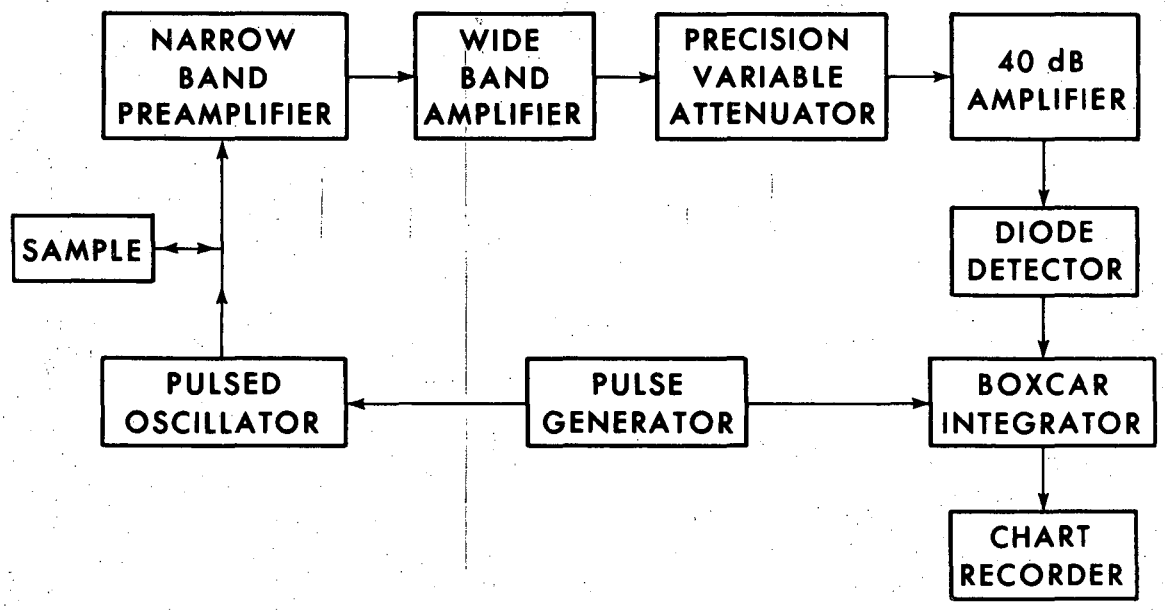

Fig. 16: Block diagram of the apparatus.

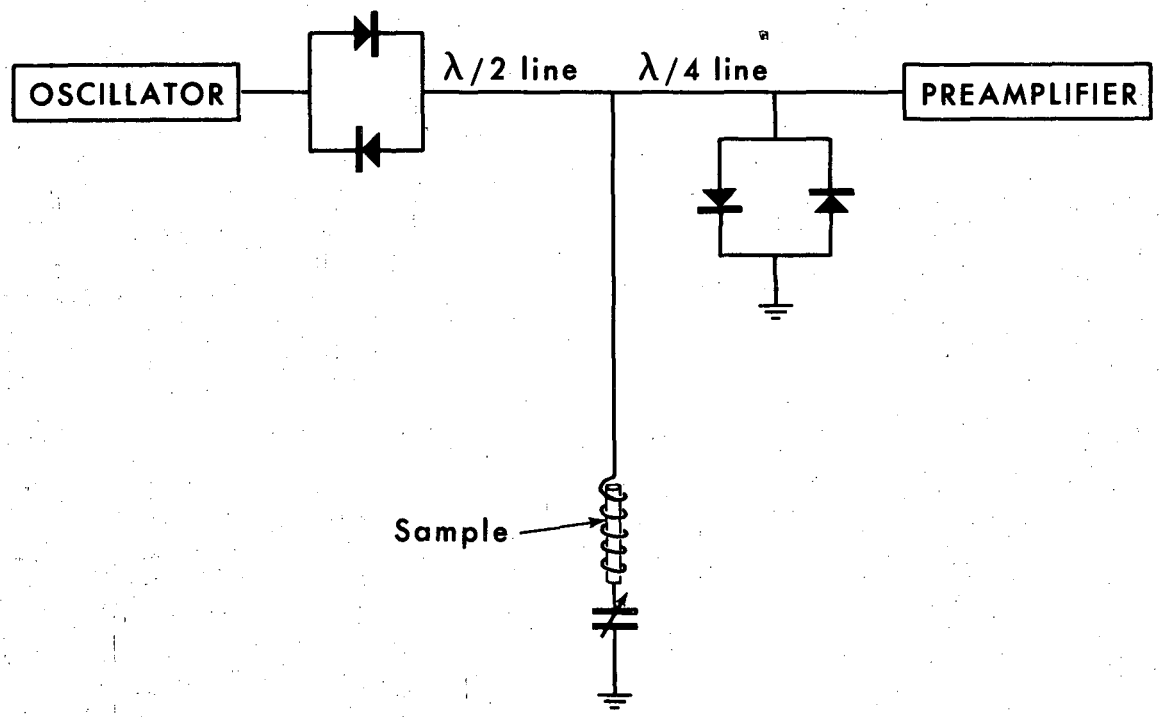

Fig. 17: Schematic illustration of the sample matching network.